Oral Presentation

137 High-throughput tomography correlated with light and electron microscopy for multi-scale imaging of human kidney tissue
Dr. Matthew Lawson[1], Alana Burrell[2], Jonas Albers[1], Xioafan Xiong[3], Virginie Uhlmann[3], Yannick Schwab[4], Candice Roufosse[5], Lucy Collinson[2], Elizabeth Duke[1]
[1]European Molecular Biology Laboratory Hamburg Unit, Hamburg, Germany, [2]The Francis Crick Institute, London, United Kingdom, [3]European Bioinformatics Institute, Cambridge, United Kingdom, [4]European Molecular Biology Laboratory, Heidelberg, Germnay, [5]Imperial College London, London, United Kingdom
223 SARS-CoV-2 and HCV infection and antiviral treatment monitored by multimodal imaging
PhD Ana Joaquina Perez-berna[1], Mr Kevin Mamprin[1], Miss Victoria Castro[2], Miss Gema Calvo[2], Mr Ricardo Valcárcel[1], Miss Eva Pereiro[1], Mr Pablo Gastaminza[2]
[1]ALBA Synchrotron, Cerdanyola del Vallès, Barcelona, Spain, [2]Centro Nacional de Biotecnología (CNB-CSIC) , Madrid, Spain
252 Linking form and function: hyperspectral and nanostructural characterisation of photonic crystals in butterflies
Professor Peta Clode[1], Anna-Lee Jessop[2], Kyle DeMarr[3], Remi Mauxion[4], Owen McMillan[4], Nipam Patel[5], Bodo Wilts[6], Gerd Schroeder-Turk[2]
[1]University of Western Australia, Perth, Australia, [2]Murdoch University, Perth, Australia, [3]University of California, Berkeley, USA, [4]Smithsonian Tropical Research Institute, Gamboa, Panama, [5]Marine Biological Laboratory, Chicago, USA, [6]University of Salzburg, Salzburg, Austria
309 Correlative imaging of the human anterior cruciate ligament by micro-CT and histology
Federica Orellana[1,2], Alberto Grassi[3], Gregorio Marchiori[3], Matteo Berni[3], Nicola Francesco Lopomo[4], Stefano Zaffagnini[3], Annapaola Parrilli[1]
[1]Empa - Center for X-ray Analytics, Dübendorf, Switzerland, [2]University of Fribourg, Fribourg, Switzerland, [3]IRCCS - Istituto Ortopedico Rizzoli, Bologna, Italy, [4]Politecnico di Milano, Milano, Italy
364 A cryo workflow combining light, electron and soft x-ray microscopy provides targeting of unlabeled features
Martin Uher[1], Sergey Kapishnikov[2], Dominik Pinkas[3], Martina Zánová[1], Kenneth Fahy[2], Samuel Zachej[1], Jakub Javurek[1]
[1]TESCAN GROUP, a.s., Brno, Czech Republic, [2]SiriusXT Ltd., Dublin, Ireland, [3]Institute of Molecular Genetics of the Czech Academy of Sciences, , Czech Republic
532 FOUR MICROSCOPY METHODS UNVEIL LIVER FENESTRATIONS: CORRELATIVE SEM, SIM, STED, AFM TARGETING SINGLE CELL TYPE
Dr Hab. Bartlomiej Zapotoczny[1], dr Karolina Szafranska[2], prof. Stefan Chlopicki[3], prof. Marek Szymonski[4], prof. Balpreet S. Ahluwalia[2], prof. Malgorzata Lekka[1], prof. Peter McCourt[2]
[1]Institute of Nuclear Physics Polish Academy of Sciences , Krakow, Poland, [2]UiT-The Arctic University of Norway, Tromsø, Norway, [3]Jagiellonian Centre for Experimental Therapeutics, Jegiellonian University , Krakow, Poland, [4]Marian Smoluchowski Institute of Physics, Jegiellonian University, Krakow, Poland
469 Microscopy techniques show the assembly of nanovesicles around lipid droplets via the tumor protein TPD54
Doctor Sandra Lacas-Gervais[1], Maud Magdeleine[2], Christelle Boscagli[1], Doctor François Orange[1], Doctor Bruno Antonny[2]
[1]Université Côte d'Azur, Centre Commun de microscopie Appliquée, CCMA, Nice, France, [2]Université Côte d'Azur, Institut de Pharmacologie Moléculaire et Cellulaire, IPMC, Valbonne, France
694 Correlative TOF-SIMS/SEM for subcellular investigation of microalgae in extreme environment
Claire Seydoux[1], Jade Ezzedine[2], Camille Beaulier[2], Grégory Si Larbi[2], Stéphane Ravanel[2], Eric Maréchal[2], Jean-Paul Barnes[3], Pierre-Henri Jouneau[1]

[1]Laboratoire Modélisation et Exploration des Matériaux, Grenoble, France, [2]Laboratoire de Physiologie Cellulaire et Végétale, Grenoble, France, [3]CEA-Leti, Grenoble, France

756 Structural remodeling of neural circuits through synthetic biological control of neuron-astrocyte interactions

Gyu Hyun Kim[1,2], Mrs. Shin Heun Kim[3], Ms. Sangkyu Lee[3], Ms. Kea Joo Lee[1]
[1]Korea Brain Research Institute, Dong-gu, Republic of Korea, [2]Korea University, Seongbuk-gu, Republic of Korea, [3]Institute for Basic Science, Yuseong-gu, Republic of Korea

818 Dual-color CLEM imaging for genetically encodable enzymatic fluorescence signal amplification method using APEX (FLEX)

Dr. Min Kyo Jung[1], Dr. Nirmali Sharma[2,3], Dr. Pratyush Kumar Mishra[2], Prof. Hyun-Woo Rhee[2,4], Dr. Ji Young Mun[1]
[1]Neural Circuits Research Group, Korea Brain Research Institute, Seoul, Korea, [2]Department of Chemistry, Seoul National University, Seoul , Korea, [3]Department of Chemistry, Ulsan National Institute of Science and Technology (UNIST), Ulsan, Korea, [4]School of Biological Sciences, Seoul National University, Seoul, Korea

819 Multimodal mechano-microscopy reveals mechanical phenotypes of breast cancer spheroids in three dimensions

Alireza Mowla[1,2], Dr Liisa Hirvonen[3], Matt Hepburn[1,2,4], Jiayue Li[1,2], Danielle Vahala[5], Sebastian Amos[5], Rowan Sanderson[1,2], Philip Wijesinghe[6], Samuel Maher[5], Yu Suk Choi[5], Brendan Kennedy[1,2,4]
[1]BRITElab, Harry Perkins Institute of Medical Research, Perth, Australia, [2]School of Engineering, The University of Western Australia, Perth, Australia, [3]Centre for Microscopy, Characterisation & Analysis (CMCA), The University of Western Australia, Perth, Australia, [4]Institute of Physics, Faculty of Physics, Astronomy and Informatics, Nicolaus Copernicus University in Toruń, Torun, Poland, [5]School of Human Sciences, The University of Western Australia, Perth, Australia, [6]Centre of Biophotonics, SUPA, School of Physics and Astronomy, University of St Andrews, St Andrews, U.K.

1067 Compartmentalization of synaptic ER studied by correlative FLIP and FIB-SEM

Dr. Helena Vihinen[1], Dr. Leena-Stiina Kontturi[2], Asst. Prof. Juha Saarikangas[2], Dr. Eija Jokitalo[1]
[1]Electron Microscopy Unit, Helsinki Institute of Life Science, Institute of Biotechnology, University of Helsinki, Helsinki, Finland, [2]Helsinki Institute of Life Science and Faculty of Biological and Environmental Sciences, University of Helsinki, , Finland

Poster Presentation

98 Multiparametric investigation of bacterial surface structure with correlative atomic force microscopy

Dr. Joan Carles Escolano[1], Torsten Müller[1], André Körnig[1], Thomas Henze[1]
[1]JPK BioAFM, Bruker Nano GmbH, Berlin, Germany

169 Correlative analytical scanning electron microscopy reveals periprosthetic tissue response to nanoparticles and wear debris

Dr Louise Hughes[1], Pedro Machado[1], Joshua Lea[1], Zhidao Xia[2]
[1]Oxford Instruments NanoAnalysis, High Wycombe, UK, [2]Swansea University, Swansea, UK

178 Combining SIMS elemental mapping with FIB-based imaging for multimodal analysis of biological specimen

Dr. Antje Biesemeier[1], Mr. Olivier de Castro[1], Miss Tatjana Taubitz[1,2], Miss Zahraa Berro[1,3], Mr Jean-Nicolas Audinot[1], Mr Tom Wirtz[1]
[1]Advanced Instrumentation for Nano-Analytics, Materials Research and Technology Department, Luxembourg Institute of Science and Technology, Belvaux, Luxembourg, [2]Department of Structural Biochemistry, Max Planck Institute of Molecular Physiology, Dortmund, Germany, [3]Doctoral Programme in Systems and Molecular Biomedicine of the DSSE, University of Luxembourg, Belval Esch-sur-Alzette, Luxembourg

402 Thapsigargin induces non-apoptotic programmed cell death in RBL-1 cells
Dr. Philip Steiner[1], Mr. Hubert Kerschbaum[2], Mrs. Ancuela Andosch[1,2], Mr. Korollus Melek[3], Mrs. Susanna Zierler[1,4]
[1]Institute of Pharmacology, Johannes Kepler University, Linz, Austria, [2]Department of Biosciences and Medical Biology, Paris Lodron University, , Austria, [3]Institute of Biochemistry and Molecular Medicine, University Bern, , Switzerland, [4]Walther Straub Institute of Pharmacology, Ludwig Maximilians University, Munich, Germany
450 Evaluation of Conventional Adherent Cell Enumeration Methodologies alongside Image-Enhanced Flow Cytometry
Dr Matthew Bourn[1], Mrs Lauren Daly[1], Mr Scott Gregory[1], Mrs Jeanne Rivera[1]
[1]National Measurement Laboratory at LGC Ltd, Leeds, UK
556 The organization of organic/biominerals in the nanostructured 3D photonic crystals in insects' scales
Dr. Yin Chang[1], Dr. Hsiang-Han Tseng[2], Dr. Luca Bertinetti[1], Dr. Michaela Wilsch-Bräuninger[3], Prof. Yael Politi[1]
[1]B CUBE - Center for Molecular Bioengineering, Technische Universität Dresden, Dresden, Germany, [2]Thermo Fisher Scientific, 1, The Felbridge Centre, Imberhorne Lane, East Grinstead, West Sussex, UK, [3]Max Planck Institute of Molecular Cell Biology and Genetics, , Germany
713 Correlative cryo soft x-ray tomography and fluorescent microscopy of biological samples in the laboratory
Mr Kenneth Fahy[1], Dr. Sergey Kapishnikov[1], Dr. Paul Sheridan[1], Mr. William Fyans[1], Dr. Fergal O'Reilly[1,2,3], Mr. Tony McEnroe[1]
[1]SiriusXT, Dublin, Ireland, [2]UCD School of Physics, Dublin 4, Ireland , [3]UCD School of Biology and Environmental Science, Dublin 4, Ireland
809 Inflammatory mechanism in Diabetes – Ultrastructural investigations of endocrine pancreas using correlative electron microscopy (STEM)
Dr. Dagmar Kolb[1,2], Bsc. Sumayya Böhm[1], Kerstin Hingerl[1], Prof. Thomas Pieber[3,4], Msc. Barbara Ehall[3,4], Bsc. Dominique Pernitsch[1], DI Lea Bogensperger[5]
[1]Core Facility Ultrastructure Analysis - Center for Medical Research, Graz, AUSTRIA, [2]Gottfried Schatz Research Center, Division of Cell Biology, Histology and Embryology, Graz, AUSTRIA , [3]Division of Endocrinology and Diabetology, Medical University of Graz, , , [4]The Center for Biomarker Research in Medicine GmbH, , , [5]Institute of Computer Graphics and Vision, Graz University of Technology, ,
826 Three-dimensional, correlative electron microscopy and immuno-labelling revealed new principles of the Golgi complex functioning
Prof. M.D.; PhD.; DcS. Alexander Mironov[1], MD, PhD, DcS Galina Beznoussenko[1]
[1]IFOM ETS—The AIRC Institute of Molecular Oncology, Milan, Italy
869 Combination of TEM, LM and micro-CT to image insects: the perspective of crop protection strategies
Nada Žnidaršič[1], Urban Bogataj[1], Polona Mrak[1], Katja Kunčič[1], Miloš Vittori[1], Primož Žigon[2], Jaka Razinger[2], Jerica Sabotič[3]
[1]University of Ljubljana, Biotechnical Faculty, Department of Biology, Ljubljana, Slovenia, [2]Agricultural Institute of Slovenia, Plant Protection Department, Ljubljana, Slovenia, [3]Jožef Stefan Institute, Department of Biotechnology, Ljubljana, Slovenia
895 Microvessel and mitochondria changes in a mouse model of Alzheimer's disease
DVM PhD Stine Hasselholt[1,2], Cagla Cömert[2,3], Jesper Just[2,4], Peter Bross[3], Jens Randel Nyengaard[1,5], Brian Hansen[2], Leif Østergaard[2]
[1]Core Centre for Molecular Morphology, Dept. of Clinical Medicine, Aarhus University, Aarhus, Denmark, [2]Center of Functionally Integrative Neuroscience, Dept. of Clinical Medicine, Aarhus University, Aarhus, Denmark, [3]Research Unit for Molecular Medicine (MMF), Dept. of Clinical Medicine, Aarhus University, Aarhus, Denmark, [4]Dept. of Molecular Medicine (MOMA), Dept. of

Clinical Medicine, Aarhus University, Aarhus, Denmark, [5]Dept. of Pathology, Aarhus University Hospital, Aarhus, Denmark

948 Human Tumor Microbiome Detection using Correlative Light and Electron Microscopy

Dr. Tali Dadosh[1], Dr. Smadar Levin-Zaidman[1], Dr. Deborah Nejman[2], Dr. Nancy Gavert[2], Prof. Ravid Straussman[2]
[1]Department of Chemical Research Support, Weizmann Institute of Science, Rehovot, Israel, [2]Department of Molecular Cell Biology, Weizmann Institute of Science, Rehovot, Israel

1095 Laboratory Soft X-ray Microscopy for Biomedical Applications

Aurélie Dehlinger[1,2], Dr. Christian Seim[1,2], Valentina Alberini[1,2], Dr. Holger Stiel[2,3], Dr. Antje Ludwig[4,5,6], Sarah Jung[1,2], Daniel Groetzsch[1,2], Vladimir Usatikov[1,2], Dr. Johannes Tuemmler[3], Prof. Dr. Birgit Kanngießer[1,2]
[1]Technische Universität Berlin, Institut für Optik und Atomare Physik, Berlin, Germany, [2]Berlin Laboratory for innovative X-ray technologies (BLiX), Berlin, Germany, [3]Max-Born-Institut (MBI) im Forschungsverbund Berlin e.V., Berlin, Germany, [4]Department of Cardiology, Angiology and Intensive Care Medicine, Deutsches Herzzentrum der Charité, Berlin, Germany, [5]Department of Cardiology, Angiology and Intensive Care Medicine, Charité - Universitätsmedizin Berlin, Corporate Member of Freie Universität Berlin and Humboldt-Universität zu Berlin, Berlin, Germany, [6]DZHK (German Centre for Cardiovascular Research), Partner Site Berlin, Berlin, Germany

Late Poster Presentation

1205 Revealing foliar nanoparticle uptake dynamics: integrating nano-CT, confocal microscopy and LA-ICP-MS insights

Phd Student Andrea Pinna[1], PhD student Emil Visby Østergaard, PostDoc Noemie Thiebaut, Professor Rajmund Mokso, Professor Søren Husted
[1]University of Copenhagen, Copenhagen, Denmark

1236 Visualization of the Endosomal Fate of mRNA-Lipid Nanoparticles Reveals the Reason for Low Escape Rate

Dr. Anke Kaltbeitzel[1], Gunnar Glaßer[1], Dr. Johanna Simon[2], Dr. Eleni Samaridou[2], Dr. Moritz Beck-Broichsitter[2], Kai Speth[1], Prof. Dr. Volker Mailänder[1], Dr. Ingo Lieberwirth[1]
[1]MPI Polymer Research, Mainz, Germany, [2]Merck KGAA, Darmstadt, Germany

1257 Correlative light electron microscopy for improved investigation of subcellular GLUT4 distribution in human skeletal muscle

PhD student, MSc Kaspar Wredstrøm Persson[1], Christian T. Voldstedlund[1], Chris Neal[3], Judith M. Mantell[2,3], Erik, A. Richter[1], Paul Verkade[2], Thomas E. Jensen[1]
[1]August Krogh Section for Molecular Physiology, Department of Nutrition Exercise and Sports, University of Copenhagen, Copenhagen, Denmark, [2]School of Biochemistry, University of Bristol, Bristol, UK, [3]Wolfson Bioimaging Facility, University of Bristol, , UK

1275 Embryonic and postembryonic development of arthropods: imaging from the cellular to the whole organism level

Polona Mrak[1], Urban Bogataj[1], Katja Kunčič[1], Žiga Fišer[1], Miloš Vittori[1], Nada Žnidaršič[1]
[1]University of Ljubljana, Biotechnical Faculty, Department of Biology, Ljubljana, Slovenia

1282 Correlative X-ray and Electron Microscopy Workflow for Investigating Grey Matter Lesions in Multiple Sclerosis

PhD Alexandra Glasmacher-Kober[1], Susann Hesse[1], Prof. Dr. Fred Wouters[1], Dr. Gertrude Bunt[1]
[1]Research Unit Innovative Microscopy Technologies, Institute for Neuropathology, University Medical Center Goettingen, Goettingen, Germany

137

High-throughput tomography correlated with light and electron microscopy for multi-scale imaging of human kidney tissue

Dr. Matthew Lawson[1], Alana Burrell[2], Jonas Albers[1], Xioafan Xiong[3], Virginie Uhlmann[3], Yannick Schwab[4], Candice Roufosse[5], Lucy Collinson[2], Elizabeth Duke[1]
[1]European Molecular Biology Laboratory Hamburg Unit, Hamburg, Germany, [2]The Francis Crick Institute, London, United Kingdom, [3]European Bioinformatics Institute, Cambridge, United Kingdom, [4]European Molecular Biology Laboratory, Heidelberg, Germnay, [5]Imperial College London, London, United Kingdom

LS-04 (1), august 29, 2024, 10:30 - 12:30

Background incl. aims
Kidney transplantation is the treatment of choice for patients with chronic kidney failure. However, rejection of the transplanted organ is still common despite immunosuppression, with antibody-mediated rejection (AMR) providing the worst prognosis, and so improving the understanding of the mechanisms of rejection is central to developing alternative therapeutics with better patient outcomes. Current imaging methods mostly rely on 2D imaging of samples using either light or electron microscopy (EM) or extremely time-consuming 3D volume EM. In this study we wanted to utilise high throughput tomography (HiTT) to non-destructively image whole hydrated tissue biopsies in fixative using X-ray imaging[1]. With HiTT we use phase-contrast imaging, which is particularly good at imaging low X-ray absorbing material such as hydrated soft tissue. Each individual scan takes 2 minutes and 16 seconds to complete with 3D reconstructions complete in 30 seconds. The speed and quality of the images allows us to:
1. Screen and target areas of interest in the kidney biopsies for both confocal microscopy targeting specific immune cells and also serial-blockface SEM (SBF-SEM).
2. We aim to correlate all the information provided across different scales to both inform on potential changes happening in AMR but to also see if the ultrastructural information from the SBF-SEM can be correlated to differences seen at the tissue level in the confocal and HiTT imaging.
3. The final long-term aim is that these cross-correlations between the three different imaging modalities can be recognised using machine learning tools to help predict whether the kidney biopsies are showing signs of AMR.

Methods
Kidney tissue biopsies (1 mm diameter punch biopsies) taken from control and transplant rejection patients (AMR-high and AMR-low) are stored in fixative (1% para-formaldehyde (PFA)). These samples are then transported to Hamburg where they are imaged using HiTT. The biopsies are mounted in small pipette tips, still in PFA, and imaged at the P14 beamline on Petra III in Hamburg. The imaging process is repeated at four distances at an energy of 18 keV, using a 10x objective (to provide a pixel size of 650 nm), with a total exposure time of 72.4 seconds for each scan. The data are then automatically reconstructed and able to be viewed in 30 seconds. For the biopsies which are several mm long we perform a vertical stitch scan which enables the whole biopsy to be imaged. Following the non-destructive 3D imaging of the whole biopsy it is returned to the Francis Crick Institute in London, here the biopsy is sectioned and prepared for confocal imaging.
Following the confocal imaging of the vibratome slices they are processed for SBF-SEM. These heavy metal stained, resin embedded slices are then re-imaged using HiTT in Hamburg at 12.7 keV and using the 20x objective (325 nm pixel size). Each of the individual slices are imaged and reconstructed in less than three minutes. The samples are then transported to EMBL Heidelberg where they are imaged using SBF-SEM. This will be targeted on regions of interest such as the glomeruli or peritubular capillaries using both the hydrated and resin embedded HiTT data. The HiTT, fluorescence

and SBF-SEM data is correlated together in MoBIE² to allow investigation of different tissue features across multiple scales. This data is segmented with a combination of manual and semi-automated processes to help generate ground-truths for training machine learning models.

Results

Here we show that whole kidney tissue biopsies from the clinic can be imaged non-destructively in 3D, as shown in figure 1 it is already possible to observe differences between the control and AMR samples. From the X-ray data alone it is possible to identify and quantify the number of glomeruli and blood vessels present in the whole biopsy as well as observe features of disease such as inflammation. In combination with the correlated confocal data taken from the same biopsy it is possible to infer specific cell types between both modalities. This vibratome section was targeted as, based on the HiTT data it was known to contain glomeruli. This can then be registered to the SBF-SEM to show changes at the ultrastructural level on targeted structures located in the X-ray imaging.

Conclusion

The High-throughput X-ray imaging provided by HiTT has facilitated the 3D imaging of whole patient biopsies at a scale and in a time frame not seen previously. This data can then be correlated with both light and electron microscopy to reveal cross-scales changes occurring in AMR.

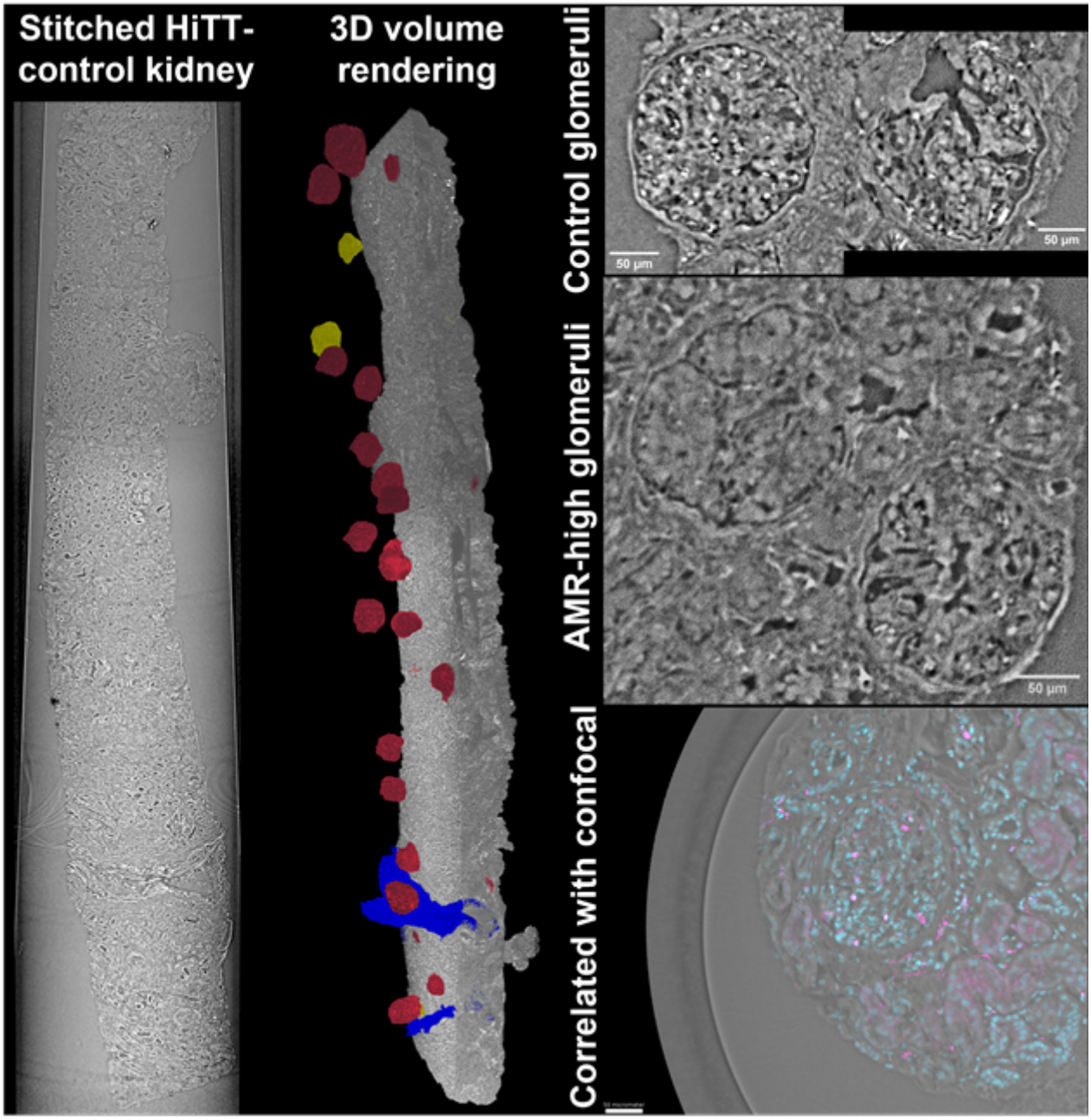

Keywords:

X-ray, Correlative, high-throughput, confocal, volume-EM

Reference:

1. Albers, J., Nikolova, M., Svetlove, A., Darif, N., Lawson, M. J., Schneider, T. R., Schwab, Y., Bourenkov, G. & Duke, E. (2024). J. Synchrotron Rad. 31, 186-194.
2. Pape, C., Meechan, K., Moreva, E. et al. MoBIE: a Fiji plugin for sharing and exploration of multi-modal cloud-hosted big image data. Nat Methods 20, 475–476 (2023)

223

SARS-CoV-2 and HCV infection and antiviral treatment monitored by multimodal imaging

PhD Ana Joaquina Perez-berna[1], Mr Kevin Mamprin[1], Miss Victoria Castro[2], Miss Gema Calvo[2], Mr Ricardo Valcárcel[1], Miss Eva Pereiro[1], Mr Pablo Gastaminza[2]
[1]ALBA Synchrotron, Cerdanyola del Vallès, Barcelona, Spain, [2]Centro Nacional de Biotecnología (CNB-CSIC) , Madrid, Spain

LS-04 (1), august 29, 2024, 10:30 - 12:30

Background
A common feature among positive strand viruses is that they alter cellular membranes to generate replication complexes. Although the origin, nature and structure of these membranous compartments are not identical, they constitute a characteristic feature of these viruses and are observed in yeast, plants and higher eukaryote (+)-strand RNA viruses (3).
HCV infection provokes a rearrangement of intracellular membranes, designated membranous web (MW). This term referred to compact vesicle accumulations embedded into a membranous matrix (2).
In SARS-CoV-2, the expression of the viral proteins results also in a profound remodeling of the infected cell cytoplasm, with the characteristic membranous compartment, generically denominated viral replication organelle (VRO). One of the salient characteristics of the coronavirus VRO is the presence of double-membrane vesicles (DMVs), where various nsp and double-stranded RNA (dsRNA) have been shown to colocalize and where active RNA-dependent RNA synthesis has been shown to occur. Thus, DMVs are the structures where coronavirus RNA replication is thought to occur. While the nature and origin of the membranes may differ, DMVs are also the putative RNA replication organelle for hepatitis C virus (HCV).
In our research we study the morphology of the membranous rearrangements induced by HCV and SARS-CoV-2 infection in near-native conditions (1).
These infection alterations in HCV could be reverted by the clinically approved direct-acting antivirals (DAAs) for the treatment of chronic HCV infection. The availability of DAA drugs against HCV provides a unique opportunity to revert this process and to define the ultrastructural events that follow viral replication blockade short after antiviral treatment (4).

Methods
In this study we have performed infrared microscopy, confocal immunofluorescence and correlative cryogenic light-soft X-ray tomography (CLXT) in the water window photon energy range to investigate in whole, unstained cells, the morphology of the membranous rearrangements induced by HCV and SARS-CoV-2 infection and after antiviral treatments in near-native conditions.

Results
Our results compare the HCV and SARS-CoV2 replicating structures. SARS-CoV-2 infected cells display DMV structures similar to those found in other coronaviruses or hepatitis C virus infection. Our studies provide a wider cellular context in which these membranous alterations occur and point at the formation of compact perinuclear structures where viral antigens are concentrated by constriction within intermediate filaments, as determined by confocal microscopy. This perinuclear structure is formed by a tightly juxtaposed tubular membranous network reminiscent of a highly modified endoplasmic reticulum. This structure is virtually devoid of normal mitochondria and adjacent mitochondria display clear ultrastructural signs of stress. Finally, late stages of the infection indicate deformation of the cell nucleus in areas close to the viral factory and an overall cytoplasmic retraction of the infected cell.

Analysis of DAA-treated HCV replicons indicate that most viral antigens and RNA are eliminated within the first 48 hours of treatment. CLXT studies confirmed the rapid elimination of the viral machinery, and the concurrent appearance of large endo-lysosomes and multivesicular bodies, suggesting a major role for this recycling machinery in the elimination of HCV-induced membranous compartments (5). A general survey of control cells and HCV replicons indicates that HCV-induced membranous alterations are no longer visible after 24 hours of treatment and that a substantial fraction of NS5A, a viral component of the replicase is located in pleomorphic, high-absorption contrast organelles in DAA-treated cells.

Conclusions

Overall, our cryo-SXT data provide an additional piece of the puzzle in building a precise map of the ultrastructure of SARS-CoV-2-infected cells by providing insight into the overall structure of the viral replication organelle and the cellular context within which these changes occur.

Our results suggest that HCV replication compartment is constantly recycled by the endo-lysosomal system and that this equilibrium is unbalanced by DAA treatment, resulting in a transient activation of the endo-lysosomal system to achieve rapid viral machinery removal. Our results also constitute a proof of concept for the use of cryo-SXT at ALBA synchrotron and at lab-scale soft X-ray microscope (SXM) as a platform that enables determining the potential impact of candidate compounds on the ultrastructure of the cell that may assist drug development at a preclinical level.

This study was funded by ALBA Synchrotron standard proposals 2022065884, 2021024899. AJPB, GC, VC, EP and PG are part of the CoCID EU project, which has received funding from the European Union's Horizon 2020 research and innovation programme under grant agreement No.1010171162. And KM is funded by CLEXM, a Marie Sklodowska-Curie Doctoral Networks Action (MSCA-DN), funded by the European Union under Horizon Europe

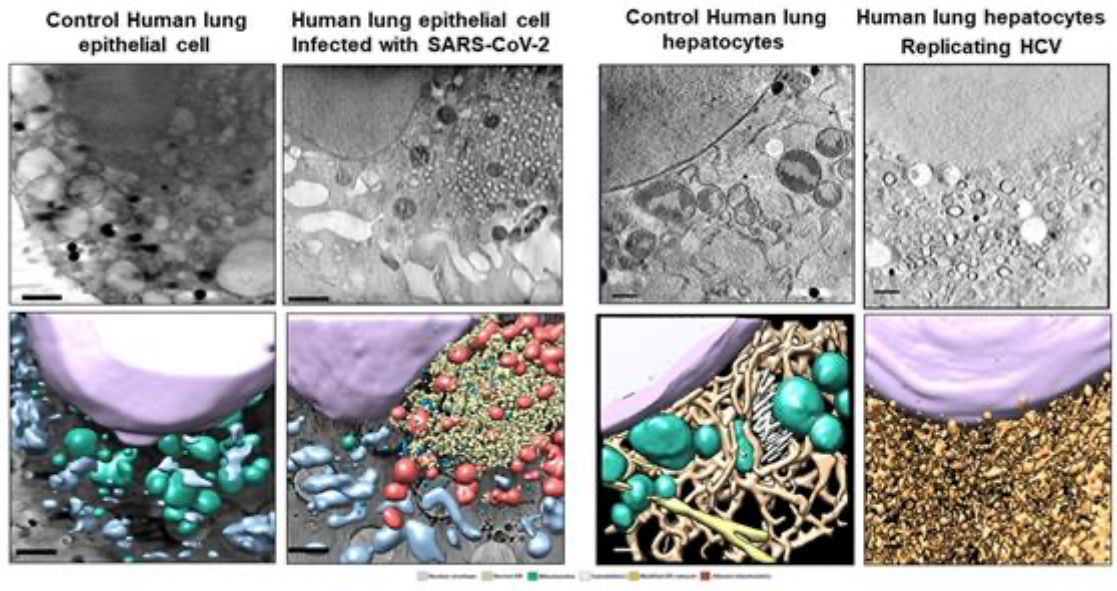

Keywords:

SARS-CoV-2, HCV, DAA, cryo-SXT,
cryogenic-light-soft-X-ray-tomography(CLXT)

Reference:

1. V Castro, AJ Pérez-Berna,et al. ACS nano 17 (22), 22708-22721
2. Pérez-Berná AJ, et al.. ACS Nano. 2016;10: 6597–6611.
3. Vasallo C, Gastaminza P. Virus Research. 2015;209: 100–117.
4. Pawlotsky J-M. Cold Spring Harb Perspect Med. 2020; a036855.
5. Perez-Berna AJ, et al. Acta Crystallogr D Struct Biol. 2021;77: 1365–1377.

252

Linking form and function: hyperspectral and nanostructural characterisation of photonic crystals in butterflies

Professor Peta Clode[1], Anna-Lee Jessop[2], Kyle DeMarr[3], Remi Mauxion[4], Owen McMillan[4], Nipam Patel[5], Bodo Wilts[6], Gerd Schroeder-Turk[2]
[1]University of Western Australia, Perth, Australia, [2]Murdoch University, Perth, Australia, [3]University of California, Berkeley, USA, [4]Smithsonian Tropical Research Institute, Gamboa, Panama, [5]Marine Biological Laboratory, Chicago, USA, [6]University of Salzburg, Salzburg, Austria

LS-04 (1), august 29, 2024, 10:30 - 12:30

Structural colour is a phenomenon whereby colour results from underlying nanostructures. For example, green colouration in the butterflies Erora opisena and Parides sesostris is a result of light interference with photonic crystals, which arrange in a single Gyroid geometry. Formation of these complex geometries and evolution of the resulting optical signals is not fully understood.

We have developed an in vivo hyperspectral microscopy technique to detect and measure optical signals emitted from wing scales of living P. sesostris pupae as they develop. Our aim is to couple these in vivo hyperspectral data with ex situ high resolution electron microscopy (SEM/TEM) and 3-dimensional imaging (3-D FIB-SEM, TEM tomography) data in order to link photonic properties to underlying nanoscale geometries of developing gyroids, over time.

Optical signals resulting from the formation of Gyroid photonic crystals begin to be emitted from the wing scales of developing pupae approximately 13 days after pupation. At this stage, a small signal peaking at ~635 nm (red) can be observed and electron microscopy confirms the onset of gyroid formation within a cellular environment. Over the next few days, the emitted spectra then increase in reflectance and the peak shifts towards shorter wavelengths by approximately 10 nm. Electron microscopy of wing scales fixed 15 days after pupation show well defined gyroid nanostructures still within a cellular environment. On emergence at ~20 days after pupation, the adult butterfly wing scales are visibly green, with gyroid formation now complete and existent in a dry state.

Due to the complex nature and length scales of these developing gyroid structures, 3-D information at the nanoscale is required to better understand their formation and development. Both FIB-SEM and TEM tomography methods offer the potential to reveal 3-D information across the nano- and micron-length scales relevant to our geometric features of interest. Preliminary FIB-SEM data reveal that we can visualise gyroid structures within wing scales of developing pupae that have been prepared using heavy metal staining and resin embedding techniques. We explore the suitability of these methods to investigate gyroid geometries in developing wing scales at time points where key shifts in optical properties have been identified with hyperspectral imaging (e.g. 13-20 days after pupation).

This multi-modal approach allows us to move toward validating mathematical modelling of simulated changes in structural geometries and functional (photonic) properties against actual structural and spectral data from developing gyroids in butterfly wing scales, over time. Such knowledge will contribute to exciting developments in fields such as synthetic biology, biomimetics, and drug delivery applications.

Keywords:

Gyroid, bicontinous structures, FIB-SEM, tomography

309

Correlative imaging of the human anterior cruciate ligament by micro-CT and histology

Federica Orellana[1,2], Alberto Grassi[3], Gregorio Marchiori[3], Matteo Berni[3], Nicola Francesco Lopomo[4], Stefano Zaffagnini[3], Annapaola Parrilli[1]
[1]Empa - Center for X-ray Analytics, Dübendorf, Switzerland, [2]University of Fribourg, Fribourg, Switzerland, [3]IRCCS - Istituto Ortopedico Rizzoli, Bologna, Italy, [4]Politecnico di Milano, Milano, Italy
LS-04 (1), august 29, 2024, 10:30 - 12:30

Background incl. aims
In case of a damage to the anterior cruciate ligament (ACL), a detailed identification of its morphological structure is essential for the biomechanically valid reconstruction of the ligament [1]. However, so far, most anatomical studies on the ACL were based on macroscopic evaluations [2] or low-resolution clinical imaging technologies (e.g. clinical computed tomography – CT, magnetic resonance imaging – MRI) [3,4]. The objective of this study was to investigate the 3D morphology of ACL in anatomical flexion and extension positions, focusing on the arrangement of its anterior and posterior fiber bundles and its femoral and tibial bone attachments. This was achieved through the correlative imaging by micro-CT, a non-destructive high resolution 3D imaging technique, and histology, leading to the identification of the four layers insertion zone of the ligament.

Methods
Healthy human knee samples (n = 2) were chemically fixed in formalin solution in knee flexion and extension and dehydrated by soaking the specimens in solutions of ascending ethanol concentration and in hexamethyldisilazane. Micro-CT analyses were carried out using an EasyTom XL Ultra 230–160 micro/nano-CT scanner (RX Solutions, Chavanod, France) with a voxel size of 17.5 µm. The generated CT datasets were analysed to create 3D models of both knees in flexion and extension using CTAn and CTVox softwares. After the micro-CT analysis, both knees were rehydrated in solutions of descending ethanol concentration, washed in distilled water, and decalcified with an aqueous solution composed of formic and nitric acid. The micro-CT 3D models were used as references to guide the orientation of the tissue for the histological analysis. Histological 5 µm thick sections were stained with hematoxylin and eosin (H&E) and Safranin O and registered, using Dataviewer software (Bruker micro-CT, Kontich, Belgium), with the corresponding orthogonal micro-CT sections.

Results
The micro-CT imaging analysis permitted the morphological 3D visualization of both soft and hard tissues of the knee in extension and flexion. These anatomical knee components were digitally identified for subsequent 3D modelling analysis, which showed a differential orientation of the ACL bundles when the knee was flexed. In particular, in the extended position the ligament exhibited a parallel course of the bundles, whereas when the knee was flexed a twisting of the bundles disrupted the parallel orientation. Direct comparison with histology permitted to identify the ACL insertion structure, comprised of four layers: ligament, fibrocartilage, mineralized fibrocartilage and bone. Moreover, this versatile method can be applied to define important joint structures, including blood vessels and nerves.

Conclusion
This study underlined the efficacy of micro-CT method to visualize the intricate anatomy of the ACL. Our protocol enabled correlative imaging using micro-CT and histology, allowing the precise assessment of ACL shape and positioning within the knee joint across different extension and flexion states. A detailed 3D description of ACL anatomy can pave the way for new regenerative medicine

and tissue engineering approaches with the aim of improving diagnostics and treatment strategies for ACL-related knee pathologies.

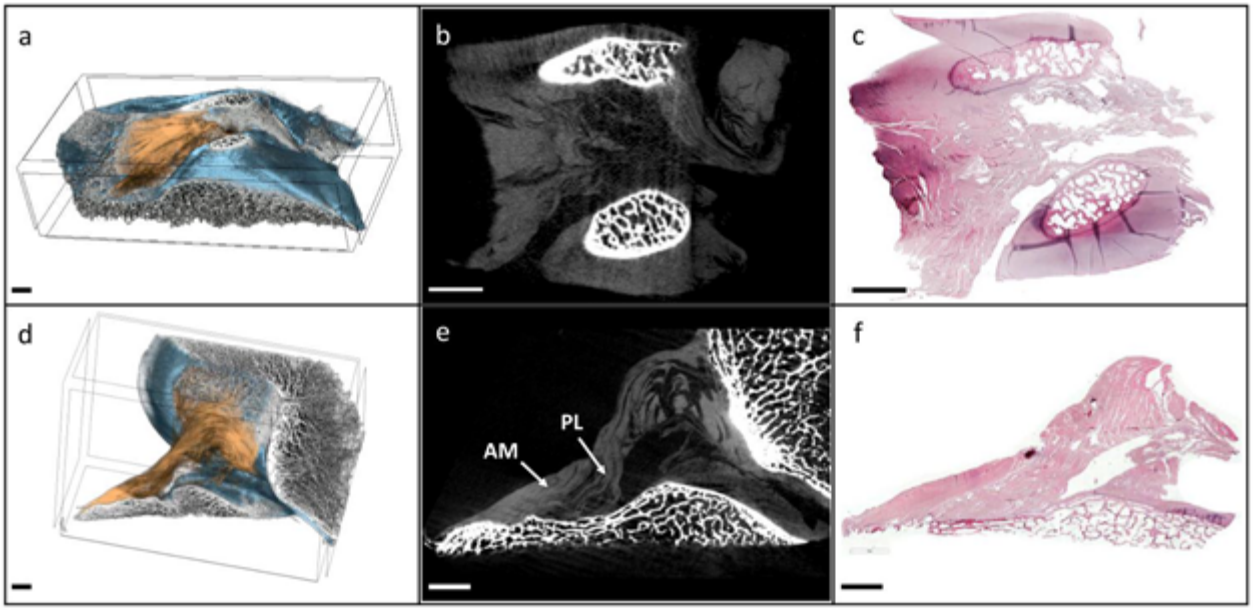

Keywords:

Micro-CT, Correlative imaging, ACL, 3D-Imaging

Reference:

[1] Grassi A, et al. (2018) SIGASCOT arthroscopy committee. New trends in anterior cruciate ligament reconstruction: a systematic review of national surveys of the last 5 years. Joints 6(3):177–187.
[2] Bicer EK, Lustig S, Servien E, Selmi TA, Neyret P (2010) Current knowledge in the anatomy of the human anterior cruciate ligament. Knee Surg Sports Traumatol Arthrosc 18(8):1075–1084.
[3] Kusano M, et al. (2017) Tibial insertions of the anterior cruciate ligament and the anterior horn of the lateral meniscus: a histological and computed tomographic study. Knee 24(4):782–791.
[4] Scheffler SU, Maschewski K, Becker R, Asbach P (2018) In-vivo three-dimensional MR imaging of the intact anterior cruciate ligament shows a variable insertion pattern of the femoral and tibial footprints. Knee Surg Sports Traumatol Arthrosc 26(12):3667–3672.
[5] Parrilli A, et al. (2024) 3D visualization of the human anterior cruciate ligament combining micro-CT and histological analysis. Surgical and radiologic anatomy 46(2): 249-258.

364

A cryo workflow combining light, electron and soft x-ray microscopy provides targeting of unlabeled features

Martin Uher[1], Sergey Kapishnikov[2], Dominik Pinkas[3], Martina Zánová[1], Kenneth Fahy[2], Samuel Zachej[1], Jakub Javurek[1]
[1]TESCAN GROUP, a.s., Brno, Czech Republic, [2]SiriusXT Ltd., Dublin, Ireland, [3]Institute of Molecular Genetics of the Czech Academy of Sciences, , Czech Republic

LS-04 (1), august 29, 2024, 10:30 - 12:30

Background incl. aims
While Electron Microscopy (EM) reveals extensive subcellular information in exquisite detail the technique has some limitations; lack of 3D cellular context, limited field of view and demanding sample preparation protocols compared to other techniques such as light or x-ray microscopy. To overcome these limitations correlative workflows have been developed that combine light with volume EM techniques such as focused ion beam scanning electron microscopy (FIB-SEM), serial block face scanning electron microscopy or array tomography, thus facilitating the localization of specific regions of interest within an extended sample volume. Nonetheless, these workflows remain largely confined to chemically fixed samples requiring labor intensive workflows, as the contrast from frozen-hydrated samples can be limited, making direct SEM imaging of native samples challenging. Soft x-ray tomography (SXT), on the other hand, is a unique x-ray imaging modality which enables imaging of frozen-hydrated specimens like entire mammalian cells or thick tissue sections with a few tens of nanometers spatial resolution and minimal sample preparation. The recent development of a laboratory scale SXT microscope opens the possibility of integrating this novel technique into light and electron imaging workflows. The SXT microscope features an integrated light microscope for overview imaging and fluorescence targeting, allows for swift acquisition of 2D and 3D images covering extensive areas on the specimen, and enables efficient and rapid identification of cells of interest. The (x,y,z) feature location can be recorded and the specimen passed to a cryo FIB-SEM for lamella extraction and subsequent cryo-ET imaging at ultra-high resolution.
Methods
Cryo SXT was used to identify target regions of interest within whole, frozen hydrated cells. Soft x-rays from 284 to 543 eV (2.34 to 4.4 nm) allow SXT to retrieve quantitative x-ray absorption information of protein content in biological cells with high native contrast. The resulting 3D datasets were imported to the correlative module in the TESCAN AMBER cryo FIB-SEM and used as a reference for targeted extraction of cryo lamella from the specimen.
Results
Resulting cryo-ET tomograms provide proof of concept for presented workflow.
Conclusion.
This workflow of correlative light, electron and soft x-ray microscopy (CLEXM) combines the strengths of both SXT and EM while also avoids any adverse effect of chemicals used for fixation in traditional EM methods, and therefore is particularly suited for studying rare events or features which cannot be labelled with fluorescent tags. We will discuss recent progress in this novel workflow development.
Acknowledgement
We acknowledge the Electron Microscopy Core Facility, IMG ASCR, Prague, CR, supported by MEYS CR (LM2018129, LM2023050, CZ.02.1.01/0.0/0.0/18_046/0016045, CZ.02.1.01/0.0/0.0/16_013/0001775).

Keywords:

CLEM, Cryo-FIB, Cryo-ET, SXT, CLEXM

532

FOUR MICROSCOPY METHODS UNVEIL LIVER FENESTRATIONS: CORRELATIVE SEM, SIM, STED, AFM TARGETING SINGLE CELL TYPE

Dr Hab. Bartlomiej Zapotoczny[1], dr Karolina Szafranska[2], prof. Stefan Chlopicki[3], prof. Marek Szymonski[4], prof. Balpreet S. Ahluwalia[2], prof. Malgorzata Lekka[1], prof. Peter McCourt[2]
[1]Institute of Nuclear Physics Polish Academy of Sciences , Krakow, Poland, [2]UiT-The Arctic University of Norway, Tromsø, Norway, [3]Jagiellonian Centre for Experimental Therapeutics, Jegiellonian University , Krakow, Poland, [4]Marian Smoluchowski Institute of Physics, Jegiellonian University, Krakow, Poland

LS-04 (1), august 29, 2024, 10:30 - 12:30

Liver sinusoidal endothelial cells (LSECs) are an excellent research target for developing high-resolution imaging methods due to their unique morphology [1]. LSEC membrane is perforated with multiple transcellular pores called fenestrations. Being in the range of 50-350 nm [2], fenestrations remain largely beyond the resolution limits of conventional optical microscopy, limited by light diffraction. LSECs play a crucial role in realizing the bidirectional transport of substances, especially lipoproteins, between blood and hepatocytes in the liver. Reduced LSEC porosity, called defenestration is often associated with ageing and chronic liver diseases such as hepatitis, steatosis, and cirrhosis. In vitro studies have shown that LSEC porosity can be altered pharmacologically [2,3]. These findings promise the development of a proper treatment allowing to reopen once closed fenestrations or to tune their diameters to achieve proper filtration properties within the liver [4]. Due to the great importance of fenestrations diameters, acting as a functional sieve for particles of a certain size into and out of the liver, the determination of the "true" fenestration size is extremely desirable.

Over the years various nanoscopy techniques have been challenged to disclose fenestrations in LSEC [5]. Obtained values of their diameters often significantly varied between the used techniques. The only way to understand these discrepancies was to visualise the exact same fenestrated areas using several techniques in a correlative manner. Each microscopy technique has its benefits and limitations originating e.g. from image acquisition, resolution, and level of sample preparation. We applied four different microscopy techniques, namely scanning electron microscopy (SEM), structured illumination microscopy (SIM), stimulated emission-depletion microscopy (STED), and atomic force microscopy (AFM), all to address the reported differences in fenestration size distribution.

A quantitative and qualitative description of the differences was made in a correlative manner [1]. Scanning electron microscopy (SEM) was combined with optical nanoscopy methods (STED, SIM). Additionally, atomic force microscopy (AFM) was used in combination with SEM (Figure) and STED, all in order to better understand the differences between literature reports on fenestration dimensions. The latter employed the prototype of a device in which AFM and STED were combined in one device, providing ease in directly overlaying obtained images. Finally, we showed the potential of correlative and comparative 4-dimensional imaging (3D + time) of living cells using AFM with fluorescence microscopy (conducted at the final stage of the experiment).
We concluded that dehydration needed in SEM causes fenestration enlargement, esspecially at the edges of so called sieve plates (Figure, arrowheads). Additionally, some fenestrations closed in hydrated samples, appear as opened after dehydration in SEM. An enlargement of fenestrations is observed when probing sample with an AFM tip if a sample is mildly fixed using formaldehyde. The effect vanishes after fixation using glutaraldehyde. The point of spread function (PSF) should be considered when calculating fenestrations from images collected using optical nanoscopy. In our hands, smallest fenestrations, below 50 nm in diameter could not be disclosed with STED nor with SIM. Thanks to correlative studies and analysis of fenestrations in a one-to-one manner, we proposed

the mathematical formula allowing for recalculation of fenestration size in order to compare data from LSEC imaged using different nanoscopy techniques. It will allow researchers to compare the results collected using different nanoscopy techniques. Finally, our results show promise of a better understanding of biological processes at the nanoscale, by combining the benefits of each method when used in a correlative way.

Research supported by the National Science Centre under the project "SYMFONIA 3", (UMO-2015/16/W/NZ4/00070), SONATA 15", (UMO-2019/35/D/NZ3/01804), and Research Council of Norway Nano2021 (288565).

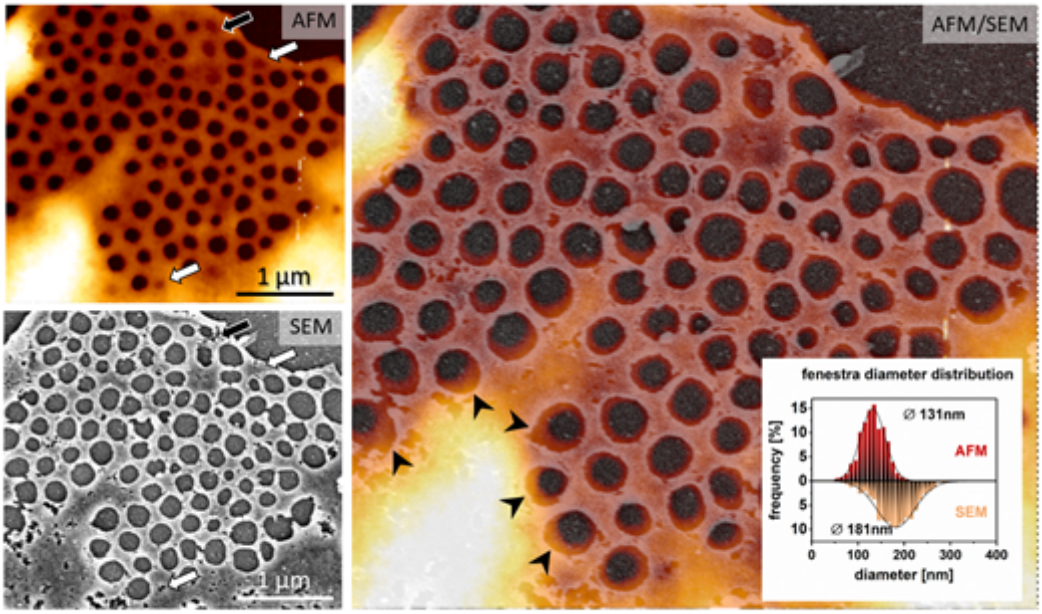

Keywords:

fenestration, liver, correlative microscopy, AFM

Reference:

[1] Szafranska K. et al., Nanophotonics, 2022. doi. 10.1515/nanoph-2021-0818;
[2] Zapotoczny B. et al., Hepatology, 2019 doi. 10.1002/hep.30232;
[3] Zapotoczny B. et al., Biophysical Reviews, 2020 doi. 10.1007/s12551-020-00699-0;
[4] Zapotoczny B. et al., International Journal of Molecular Sciences, 2022, doi: 10.3390/ijms23179850
[5] Szafranska K. et al., Frontiers in Physiology, 2021 doi. 10.3389/fphys.2021.735573

469

Microscopy techniques show the assembly of nanovesicles around lipid droplets via the tumor protein TPD54

Doctor Sandra Lacas-Gervais[1], Maud Magdeleine[2], Christelle Boscagli[1], Doctor François Orange[1], Doctor Bruno Antonny[2]
[1]Université Côte d'Azur, Centre Commun de microscopie Appliquée, CCMA, Nice, France, [2]Université Côte d'Azur, Institut de Pharmacologie Moléculaire et Cellulaire, IPMC, Valbonne, France

LS-04 (2), august 29, 2024, 14:00 - 16:00

Background : TPD54 belongs to the TPD52-like family of tumor proteins which are of great interest because they are overexpressed in aggressive metastatic cancers with poor prognosis. Recently an article showed the membrane association of TPD54 with small vesicles of around 30 nm, half the size of conventional transport vesicles, and its involvement in cell migration (1). To determine the underlying mechanism, our collaborators showed that this protein has an ALPS motif (Amphipathic lipid packing sensor), which recognizes curved membranes, and binds nanovesicles via ALPS-dependent and -independent mechanisms (2). However, its functions remain unclear. To further understand the function of TPD54 in intracellular trafficking, we worked on cultures of epithelial cells (RPE1) overexpressing various forms of GFP-TPD54, including phospho-mimetic mutants.
Methods : By confocal microscopy, the localisation of the two mutants GFP-TPD54 S166E and S166A was analyzed. A cell ultrastructural analysis was realized by different transmission electron microscopy (TEM) methods and correlative light and electron microscopy (CLEM) techniques: a) classical chemical fixation and epon embedding, and tomography b) Tokuyasu immunogold TPD54-GFP localization, c)CLEM on HM20 resin sections on samples prepared with high pressure freezing, and freeze substitution in uranyl acetate 0,2%. Sections were observed with a JEOL 1400 TEM.
Results : Confocal microscopy shows that GFP-TPD54 phosphomimetic S166E is localized to Golgi apparatus, whereas GFP-TPD54 S166A is also found at big spherical structures at the periphery of the nucleus and colocalized with Rab11, a small G protein associated to recycling endosomes. The GFP fluorescence is also found around lipid droplets. When overexpressed in RPE1 cells, we observed by TEM that TPD54 induces the formation of huge assemblies of very small vesicles and tubular structures in close contact but still at a defined distance (10-20 nm) from lipid droplets. The diameter of the vesicles (38 +/- 8 nm) is about half the size of classical transport vesicles (e.g. COPI and COPII vesicles). These assemblies contain selective membrane markers including the autophagy transmembrane protein ATG9 and RAB11. The immunogold staining and CLEM confirm the localization of TPD54 to the vesicular aggregates.
Conclusion: Our EM observations validate the existence of the TPD54 nanovesicles without the artificial trick of mitochondrial attachment published previously by Larocque et al. Furthermore, they suggest an intimate link with lipid droplets. This process seems controlled by phophorylation.

Keywords:

Electron Microscopy, nanovesicles, CLEM, TPD54

Reference:

(1) G. Larocque , D. J Moore , M. Sittewelle , C. Kuey , J. H R Hetmanski , P. J La-Borde , B. J Wilson , N. I Clarke, P. T Caswell, S. J Royle . Intracellular nanovesicles mediate α5β1 integrin trafficking during cell migration J Cell Biol. 2021 Oct 4;220(10).
(2) A. Reynaud, M. Magdeleine, A. Patel , A-S. Gay, D. Debayle, S. Abelanet, B. Antonny. Tumor protein D54 binds intracellular nanovesicles via an extended amphipathic region. J Biol Chem . 2022 Jul;298(7):102136. doi: 10.1016/j.jbc.2022.102136.

694

Correlative TOF-SIMS/SEM for subcellular investigation of microalgae in extreme environment

Claire Seydoux[1], Jade Ezzedine[2], Camille Beaulier[2], Grégory Si Larbi[2], Stéphane Ravanel[2], Eric Maréchal[2], Jean-Paul Barnes[3], Pierre-Henri Jouneau[1]
[1]Laboratoire Modélisation et Exploration des Matériaux, Grenoble, France, [2]Laboratoire de Physiologie Cellulaire et Végétale, Grenoble, France, [3]CEA-Leti, Grenoble, France

LS-04 (2), august 29, 2024, 14:00 - 16:00

Visualizing the metabolism within its structural context is key to understanding the biological phenomena at stake, especially at the subcellular scale. While biochemical purification may function for specific organelles of model species, this is tedious and often impossible for atypical or less studied organisms. Time-of-flight secondary ion mass spectrometry (TOF-SIMS) enables the combined visualization of elements and molecules and is becoming more and more popular in the field of life sciences, especially for the investigation of tissue samples. Even though the ultimate lateral resolution of TOF-SIMS ought to be sufficient for subcellular imaging, very few studies have yet pushed the lateral resolution that far. In this context, we have investigated how the subcellular architecture and molecular composition of microalgae thriving in extreme environments is affected by the harsh conditions they live in.
For this purpose, we have performed TOF-SIMS imaging, combining both high lateral resolution (up to 100 nm) and high mass resolution (up to 9,000) over resin-embedded specimen. We also performed over the same zone correlative SEM (10 nm) in order to identify subcellular compartments and used this image to segment the hyperspectral TOF-SIMS dataset. We are thus combining the strength of both techniques and increasing the resolution of TOF-SIMS imaging using SEM-derived information.
We investigated the snow alga Sanguina nivaloides that blooms over lasting snow in the spring season and was recently been identified in the Alps, as well as the uranium-tolerant Coelastrella sp. PCV that has been shown to tolerate extremely high doses of uranium. In these algae, we have been able to perform molecular profiling of several subcellular features, including cell walls as thin as ~ 100 nm, nuclei, pyrenoid, starch granules and platelets and chloroplasts. In the case of S. nivaloides especially, the environmental samples hint at a likely interaction between the alga, mineral particles and bacteria that could explain how the alga is able to collect micronutrients in its hostile snow environment. Coelastrella on the other hand is able to remodel its compartments and their metabolic content when submitted to uranium-related stress.
Our TOF-SIMS images almost meet NanoSIMS images (that is however restricted to purely elemental mass spectrometry imaging) in term of resolution. Correlative TOF-SIMS/SEM allows a remarkable enhancement of the comprehensibility of TOF-SIMS images by adding in extra structural information. We reveal for every different organelle a different metabolic footprint and hints into their adaption to their specific environment.

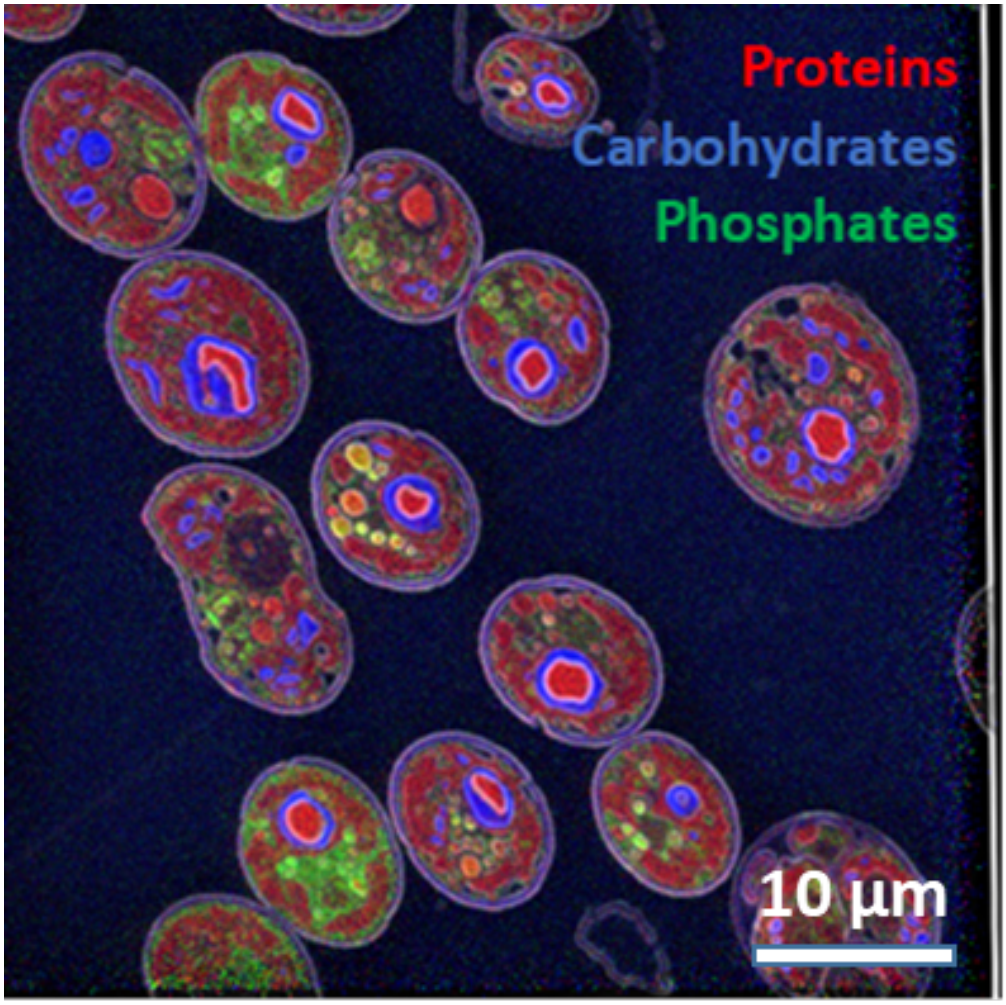

Keywords:

Metabolic imaging, Microalgae, Correlative microscopy

Reference:

Ezzedine, Jade A., et al. "Adaptive traits of cysts of the snow alga Sanguina nivaloides unveiled by 3D subcellular imaging." Nature Communications 14.1 (2023): 7500.
Beaulier, Camille, et al. "Characterization of a uranium-tolerant green microalga of the genus Coelastrella with high potential for the remediation of metal-polluted waters." Science of The Total Environment 908 (2024): 168195.

emc2024 COPENHAGEN

756

Structural remodeling of neural circuits through synthetic biological control of neuron-astrocyte interactions

Gyu Hyun Kim[1,2], Mrs. Shin Heun Kim[3], Ms. Sangkyu Lee[3], Ms. Kea Joo Lee[1]
[1]Korea Brain Research Institute, Dong-gu, Republic of Korea, [2]Korea University, Seongbuk-gu, Republic of Korea, [3]Institute for Basic Science, Yuseong-gu, Republic of Korea

LS-04 (2), august 29, 2024, 14:00 - 16:00

Background incl. aims
In the adult hippocampus, synaptic plasticity is essential for information processing, learning, and memory formation. Astrocytes, the most common type of glial cells, play pivotal roles in synapse formation, maintenance, and elimination. However, our understanding and manipulation of complex interactions between neurons and astrocytes are just the beginning.
Methods
Here, we present a synthetic approach for synapse elimination via engineering of direct neuro-glial interactions which result in the uptake of synaptic components by astrocytes. Trogocytosis is a process in which a cell takes up a portion of another cell's membrane and internalizes it. Induced synthetic trogocytosis, the uptake of ligand-labeled membrane fragments by receptor-expressing cells, has the property of unidirectional molecular transfer. We assessed potential structural changes induced by engineered neuron-astrocyte interactions using 3D correlative light and electron microscopy (CLEM) and array tomograhy.
Results
Our results provided clear evidence for the partial capture and elimination of presynaptic boutons and axons in ligand-expressing CA3 neurons by receptor-expressing astrocytes in the CA1 area. Notably, astrocytes mainly engulfed partial axonal debris or small vesicles at the initial stage of viral expression, while they later swallowed up larger presynaptic materials including mitochondria.
Conclusion
This approach will provide an insight into how the brain adaptively shapes neural circuits upon synapse elimination and offer a versatile means to structurally modulate cell-cell connections.

Keywords:

synthetic trogocytosis, neuro-glia interaction, neural-circuits

818

Dual-color CLEM imaging for genetically encodable enzymatic fluorescence signal amplification method using APEX (FLEX)

Dr. Min Kyo Jung[1], Dr. Nirmali Sharma[2,3], Dr. Pratyush Kumar Mishra[2], Prof. Hyun-Woo Rhee[2,4], Dr. Ji Young Mun[1]
[1]Neural Circuits Research Group, Korea Brain Research Institute, Seoul, Korea, [2]Department of Chemistry, Seoul National University, Seoul , Korea, [3]Department of Chemistry, Ulsan National Institute of Science and Technology (UNIST), Ulsan, Korea, [4]School of Biological Sciences, Seoul National University, Seoul, Korea

LS-04 (2), august 29, 2024, 14:00 - 16:00

Background
Correlative Light and Electron Microscopy (CLEM) is a useful imaging approach that allows us to obtain two types of different imaging information from the same sample. Fluorescence microscopy (FM) provides multi-color information on different proteins of interest (POIs), while electron microscopy (EM) reveals the ultrastructure of cellular organelles. As a result, CLEM, which has become an essential tool in cell biology and neuroscience, enables a comprehensive understanding of POIs and their connections to intracellular structures or subcellular organelles1,2. For fluorescence-mediated visualization of intracellular regions of interest, fluorescent proteins (FPs) are commonly used. However, the fluorescence of intracellular FPs is often lost, especially during harsh EM sample preparation, such as fixation, dehydration, heating and resin embedding3. Especially for highly dynamic organelles such as mitochondria and lysosomes, the precise localization of these organelles can change as they are observed live in the light microscope and are actively moving even during the short delay time for fixation. To overcome this problem, we developed a fluorescent reporter that can effectively maintain its fluorescence signal under harsh EM sample processing conditions and developed a method to obtain distortion-free CLEM images using it.

Methods
Given the difficulty of maintaining the fluorescence signal during EM sample preparation with conventional fluorescent proteins, we use a two-colour CLEM technique that integrates small molecule probe-based signal amplification using genetically encoded peroxidases with mEosEM4, which retains fluorescence even in strong fixatives. In particular, based on our previous findings on peroxidase-based fluorescent substrates, we synthesised and applied to CLEM imaging a newly designed JF-induced probe based on the styryl-benzothiazolium phenol probe genfluor (JF), known for its fluorescent signal amplification by peroxidase5.

Results
As a results, we developed a fluorescent probe (JFT1) that exhibits a fluorescence-amplified signal when APEX2 is expressed. Unlike conventional fluorescent labels or fluorescent proteins that lose their fluorescence upon OsO4 pretreatment, JFT1 produces a well-retained and restricted fluorescence pattern in both OsO4 pretreated and OsO4 post-treated samples. The application of FLEX targeting to lysosomes in conjunction with mito-mEosEM facilitated the visualization of interactions between lysosomes and mitochondria. It also revealed distinct contacts between these two organelles in response to the lysosomal stressors bafilomycin and U18666A. Furthermore, the interactions observed under the influence of bafilomycin and U18666A revealed distinct mechanisms of action as indicated by CLEM imaging. Taken together, we propose that our FLEX approach is a very

useful way to target different APEX-POI combinations for fluorescence and high-resolution EM imaging.

Keywords:

CLEM. APEX, Proximity-labeling, Fluorescent probe

Reference:

1. Paez-Segala, M., Sun, M., Shtengel, G. et al. Fixation-resistant photoactivatable fluorescent proteins for CLEM. Nat Methods 12, 215–218 (2015). https://doi.org/10.1038/nmeth.3225
2. Tanida, I., Furuta, Y., Yamaguchi, J. et al. Two-color in-resin CLEM of Epon-embedded cells using osmium resistant green and red fluorescent proteins. Sci Rep 10, 21871 (2020). https://doi.org/10.1038/s41598-020-78879-x
3. Joosen, L., Hink, M. A., Gadella, T. W., Jr. & Goedhart, J. Effect of fixation procedures on the fluorescence lifetimes of Aequorea victoria derived fluorescent proteins. J Microsc. 256 (3), 166-176, doi:10.1111/jmi.12168, (2014).
4. Fu, Z., Peng, D., Zhang, M. et al. mEosEM withstands osmium staining and Epon embedding for super-resolution CLEM. Nat Methods 17, 55–58 (2020). https://doi.org/10.1038/s41592-019-0613-6
5. Krieg R, Halbhuber KJ. Detection of endogenous and immuno-bound peroxidase--the status quo in histochemistry. Prog Histochem Cytochem. 2010 Jun;45(2):81-139. doi: 10.1016/j.proghi.2009.11.001. Epub 2010 Feb 26. PMID: 20488278.

819

Multimodal mechano-microscopy reveals mechanical phenotypes of breast cancer spheroids in three dimensions

Alireza Mowla[1,2], Dr Liisa Hirvonen[3], Matt Hepburn[1,2,4], Jiayue Li[1,2], Danielle Vahala[5], Sebastian Amos[5], Rowan Sanderson[1,2], Philip Wijesinghe[6], Samuel Maher[5], Yu Suk Choi[5], Brendan Kennedy[1,2,4]
[1]BRITElab, Harry Perkins Institute of Medical Research, Perth, Australia, [2]School of Engineering, The University of Western Australia, Perth, Australia, [3]Centre for Microscopy, Characterisation & Analysis (CMCA), The University of Western Australia, Perth, Australia, [4]Institute of Physics, Faculty of Physics, Astronomy and Informatics, Nicolaus Copernicus University in Toruń, Torun, Poland, [5]School of Human Sciences, The University of Western Australia, Perth, Australia, [6]Centre of Biophotonics, SUPA, School of Physics and Astronomy, University of St Andrews, St Andrews, U.K.

LS-04 (2), august 29, 2024, 14:00 - 16:00

Background incl. aims

Cancer cell invasion relies on an equilibrium between cell deformability and the biophysical constraints imposed by the extracellular matrix (ECM), and multicellular spheroids are a powerful model to study biochemical and biophysical interactions between cancer cells during growth and progression. However, little is known about how the biomechanics of the three-dimensional (3D) tumour microenvironment (TME) control cancer cell behaviours. 3D TME models remain underutilised, because contemporary mechanical quantification tools are limited to surface measurements, and there is a lack of enabling technologies that can measure subcellular-scale elasticity and co-register it with the morphology and function of cells in a 3D microenvironment.

Here, we develop a multimodal mechano-microscopy system that integrates optical coherence microscopy-based elasticity imaging with confocal fluorescence microscopy. We use this multimodal microscope to quantify local mechanics of cancer cell spheroids in 3D TMEs.

Methods

Our multimodal mechano-microscopy setup integrates high-resolution interferometric detection of optical coherence microscopy (OCM), a high-resolution variant of optical coherence tomography (OCT), with compression elastography and confocal fluorescence microscopy.[1] The system utilises a supercontinuum laser, whose output was shaped to a spectral range of 650 nm to 950 nm. This spectrum corresponded to a full-width at half-maximum (FWHM) bandwidth of ~250 nm, providing a measured OCM axial resolution of 1.4 µm in air. The system was implemented as a Michelson interferometer in a dual-arm configuration with the same optics in the reference beam path to match optical dispersion. The sample arm beam was expanded to fill the entrance pupil of a 20X 0.75NA objective lens providing a measured lateral resolution of 0.5 µm. Scanning was achieved using a 2D galvanometer system. A spectrometer comprising a 2048-pixel line camera was used to detect the spectral interference at each xy location.

The integrated confocal fluorescence microscope comprised two laser lines at 405 nm and 488 nm for excitation and a photomultiplier tube as the detector. The confocal system used the same galvanometer scanning arm and optics as the OCM system to scan the focal point in the sample. The emitted fluorescence from the sample was focused into a multi-modal optical fibre, which also acted as the confocal pinhole. The measured lateral resolution of the confocal imaging system was 0.5 µm, and the axial resolution ~8 µm.

Sample preparation is described elsewhere in more detail [1]. Briefly, MCF-7 and MDA-MB-231 cells were suspended in gelatin methacryloyl (GelMA) solution. The solution was pipetted into moulds placed on glass slides, and exposed to UV light for 15 or 60 s to produce soft and stiff gels, respectively. The cells were then cultured for 6-16 days to allow spheroid formation and growth. Prior to imaging, the cells were labelled with nuclear dye Hoechst 33342 and membrane dye CellMask Green for fluorescence microscopy.

For imaging, the gel sample with a thickness of ~400–500 µm and a 1 mm thick compliant silicone layer were compressed between the coverslip and a rigid optical window attached to an annular piezoelectric actuator (Fig 1a). Two B-scans were acquired at each y-location, one at the unloaded and the other at the loaded state. Local displacement was calculated from the phase difference between the two B-scans and strain was estimated as the gradient of the axial displacement with depth.[2] Strain in the layer was related to stress through knowledge of the stress–strain response of the compliant layer in contact with the sample. Confocal images were acquired directly after the mechano-microscopy measurement.

Results

To test the setup, Young's modulus of blank, soft and stiff gelatin methacryloyl (GelMA) samples was first measured using mechano-microscopy and was found to be in good agreement with AFM surface measurement (Fig 1b). The multimodal setup was then used to obtain volumetric maps of living breast cancer cell spheroids cultured in the gels. Fig 1c,d shows example en face and B-scan Young's modulus of a non-metastatic spheroid, and Fig 1e-g show an example of a volumetric map where (e) OCM intensity, (f) Young's modulus and (g) confocal fluorescence image of the nuclear (cyan) and membrane (red) fluorescent dyes.

By imaging both metastatic (MCF-7) and non-metastatic (MDA-MB-231) breast cancer cell spheroids cultured in both soft and stiff gels ($n \geq 4$ for each condition), we observe that non-metastatic cancer spheroids show no invasion while showing increased peripheral cell elasticity in both stiff and soft environments. Metastatic cancer spheroids, however, show ECM-mediated softening in a stiff microenvironment and, in a soft environment, initiate cell invasion with peripheral softening associated with early metastatic dissemination. This exemplar of live-cell 3D mechanotyping supports that invasion increases cell deformability in a 3D context, illustrating the power of multimodal mechano-microscopy for quantitative mechanobiology in situ.

Conclusion

We demonstrate a multimodal imaging system that integrates an OCM-based subcellular mechano-microscopy system with a multi-channel confocal fluorescence microscopy system. This multimodal mechano-microscopy presents a new opportunity for quantifying local Young's modulus in live 3D samples with subcellular resolution, directly revealing mechanical phenotypes in situ.

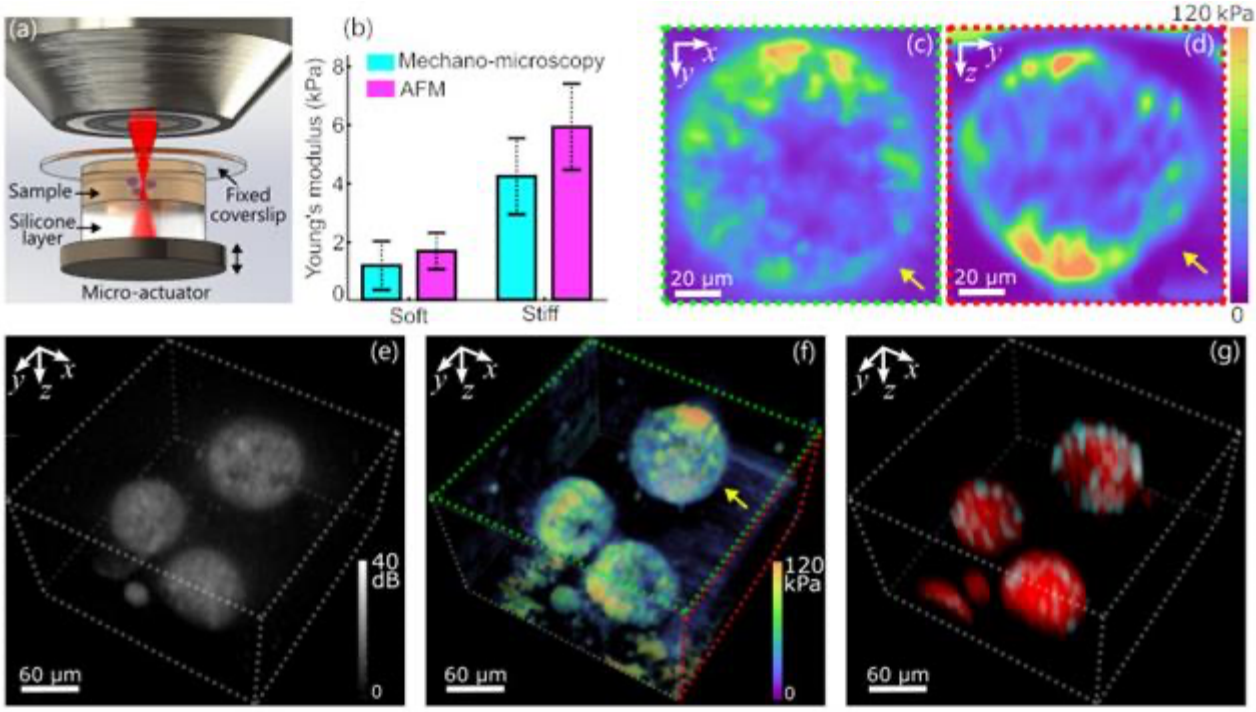

Keywords:

Multimodal microscopy, elastography, OCM

Reference:

[1] A. Mowla, . S. Hepburn, J. Li, D. Vahala, S. E. Amos, L. M. Hirvonen, R. W. Sanderson, P. Wijesinghe, S. Maher, Y. S. Choi, B. F. Kennedy, “Multimodal mechano-microscopy reveals mechanical phenotypes of breast cancer spheroids in three dimensions”, bioRxiv 2024.04.05.588260 (2024), doi: https://doi.org/10.1101/2024.04.05.588260

[2] A. Mowla, J. Li, M. S. Hepburn, S. Maher, L. Chin, G. C. Yeoh, Y. S. Choi, and B. F. Kennedy, “Subcellular mechano-microscopy: high resolution three-dimensional elasticity mapping using optical coherence microscopy” Opt. Lett. 47(13), 3303-3306 (2022).

1067

Compartmentalization of synaptic ER studied by correlative FLIP and FIB-SEM

Dr. Helena Vihinen[1], Dr. Leena-Stiina Kontturi[2], Asst. Prof. Juha Saarikangas[2], Dr. Eija Jokitalo[1]
[1]Electron Microscopy Unit, Helsinki Institute of Life Science, Institute of Biotechnology, University of Helsinki, Helsinki, Finland, [2]Helsinki Institute of Life Science and Faculty of Biological and Environmental Sciences, University of Helsinki, , Finland

LS-04 (2), august 29, 2024, 14:00 - 16:00

In hippocampal pyramidal cells, the endoplasmic reticulum (ER) comprises of small sheets connected with tubular network spreading to the tip of the axons and dendritic branches where it participates in the local protein synthesis required for synaptic transmission. The ER is known to be present in some of the dendritic protrusions called spines and it is highly dynamic in nature (Breit et al., 2018, Konietzny et al., 2023). In large spines, the ER forms a specialized organelle, the spine apparatus whereas in smaller spines the ER can comprises only one single ER tubule. Thousands of spines protruding from a single neuron differ morphologically and functionally from each other. To response to activation independently, each spine is supposed to have a distinct microenvironment e.g., the concentration of calcium ions differs from that in the dendrite and other spines (Breit et al., 2018). The spine morphology supports the compartmentalization, however other mechanisms are needed to obtain unidirectional diffusion and separated environment. The aim of this research was to substantiate whether the synaptic ER can be compartmentalized in the dendritic spines.

To study the compartmentalization of the synaptic ER, primary hippocampal neurons were cultivated on etched cover slips and transiently transfected with fluorescence markers for the ER and cytoplasm. The target dendrite was subjected to FLIP (fluorescence loss in photobleaching) where a part of the dendrite was bleached by pulsed light and the amount of fluorescence at the target spines after each pulse was detected. After FLIP the samples were chemically fixed and prepared for FIB-SEM (focused ion beam scanning electron microscopy). The target areas imaged with light microscope were correlated in FIB-SEM using a back scattered electron detector and the datasets were collected using 6 or 8 nm isotropic pixels. The dendrites in the FIB-SEM datasets were modelled using semi-automated segmentation tools in Microscopy Image Browser software (MIB, Belevich et al., 2016).

The FLIP studies indicated that the ER proteins may be in compartments closed off from the rest of the dendrite, preventing them from being affected by the repeated photobleaching. FIB-SEM applied to the correlated spines confirmed the results and revealed a subset of the non-continuous, compartmentalized synaptic ER. A single continuing ER tubule in a synaptic spine may have a diameter ca. 20 nm, however the volume-EM was required to enable the pinpointing the target spine in the complex neuronal network. In addition to compartmentalized synaptic ER, FIB-SEM data revealed variety of different shapes and size of dendritic spines as well as ER with two different densities. The ER with clearly different density joined and emerged throughout the whole volume of dendrites and even in some of the synaptic spines. No protein coat (possibly septin protein) could be detected around the spine neck, however, some of the spines with compartmentalized synaptic ER had a very long and narrow neck.

As a conclusion it can be said that correlative FLIP and FIB-SEM is a powerful tool to study temporally and spatially rare event in cell cultures and it allows to analyze the structures like a single tubular ER in a large neuronal network. Applying correlative FLIP and FIB-SEM verified the compartmentalization of the ER in a subset of synaptic spines. More studies must be done to further elucidate

compartmentalization of the synaptic ER and its role in maintaining of synaptic strength and supporting neuronal function and plasticity.

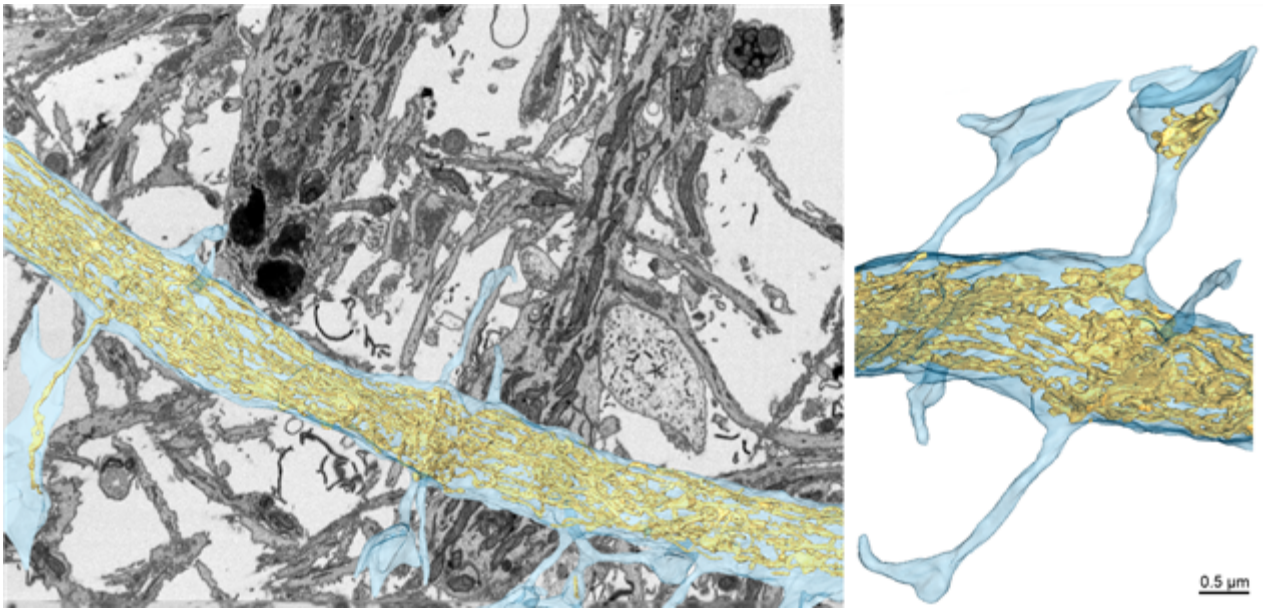

Keywords:

CLEM, FIB-SEM, FLIP, volume-EM, ER

Reference:

Belevich I, Joensuu M, Kumar D, Vihinen H, Jokitalo E. Microscopy Image Browser: A Platform for Segmentation and Analysis of Multidimensional Datasets. PLoS Biol. 2016 Jan 4;14(1):e1002340. doi: 10.1371/journal.pbio.1002340. PMID: 26727152; PMCID: PMC4699692.

Breit M, Kessler M, Stepniewski M, Vlachos A, Queisser G. Spine-to-Dendrite Calcium Modeling Discloses Relevance for Precise Positioning of Ryanodine Receptor-Containing Spine Endoplasmic Reticulum. Sci Rep. 2018 Oct 23;8(1):15624. doi: 10.1038/s41598-018-33343-9. PMID: 30353066; PMCID: PMC6199256.

Konietzny A, Wegmann S, Mikhaylova M. The endoplasmic reticulum puts a new spin on synaptic tagging. Trends Neurosci. 2023 Jan;46(1):32-44. doi: 10.1016/j.tins.2022.10.012. Epub 2022 Nov 22. PMID: 36428191.

98

Multiparametric investigation of bacterial surface structure with correlative atomic force microscopy

Dr. Joan Carles Escolano[1], Torsten Müller[1], André Körnig[1], Thomas Henze[1]
[1]JPK BioAFM, Bruker Nano GmbH, Berlin, Germany

Poster Group 2

Background incl. aims
Atomic force microscopy (AFM) has become an indispensable tool for high-resolution structural analysis of specimens ranging from single molecules to complex biological systems, while simultaneously being able to correlate topography and mechanics at near native/physiological imaging conditions. In turn, the combination with advanced/customized optics leverages the advantages of immunolabelling techniques for truly correlative microscopy. Specifically, the use of a tip-scanning AFM, as compared to a sample-scanning system, enables simultaneous high-resolution correlation experiments with advanced optical techniques. Studying certain Gram(-) bacterial species have attracted a lot of interest recently as model systems for investigating their outer membrane envelope.

Methods
We have applied fast tip-scanning AFM imaging in combination with confocal microscopy to study the surface structure of bacterial species. We have studied the surface structure of E. coli MG1655 bacteria to gain a deeper insight into the supramolecular organization of their outer membrane protein network.

Results
By additionally exploiting full-fledged sample mechanical mapping we can correlate any substructural surface analysis of the layered bacterial specimen with differences in bacterial stiffness. We demonstrate how the application of dual z-actuator tip-scanning AFM imaging can be exploited for instant high-resolution analysis of tall bacterial samples exceeding 1 µm in height. We will also discuss how the combination of high-speed tip-scanning AFM with antimicrobial agents can be used as a tool to study the bacterial envelope in real-time and potentially develop strategies for fighting microbial resistance.

Conclusion
AFM can be successfully applied to correlate high-resolution structural features and mechanical properties of the outer membrane envelope in MG1655 E. coli bacterial species in combination with advanced optical microscopy.

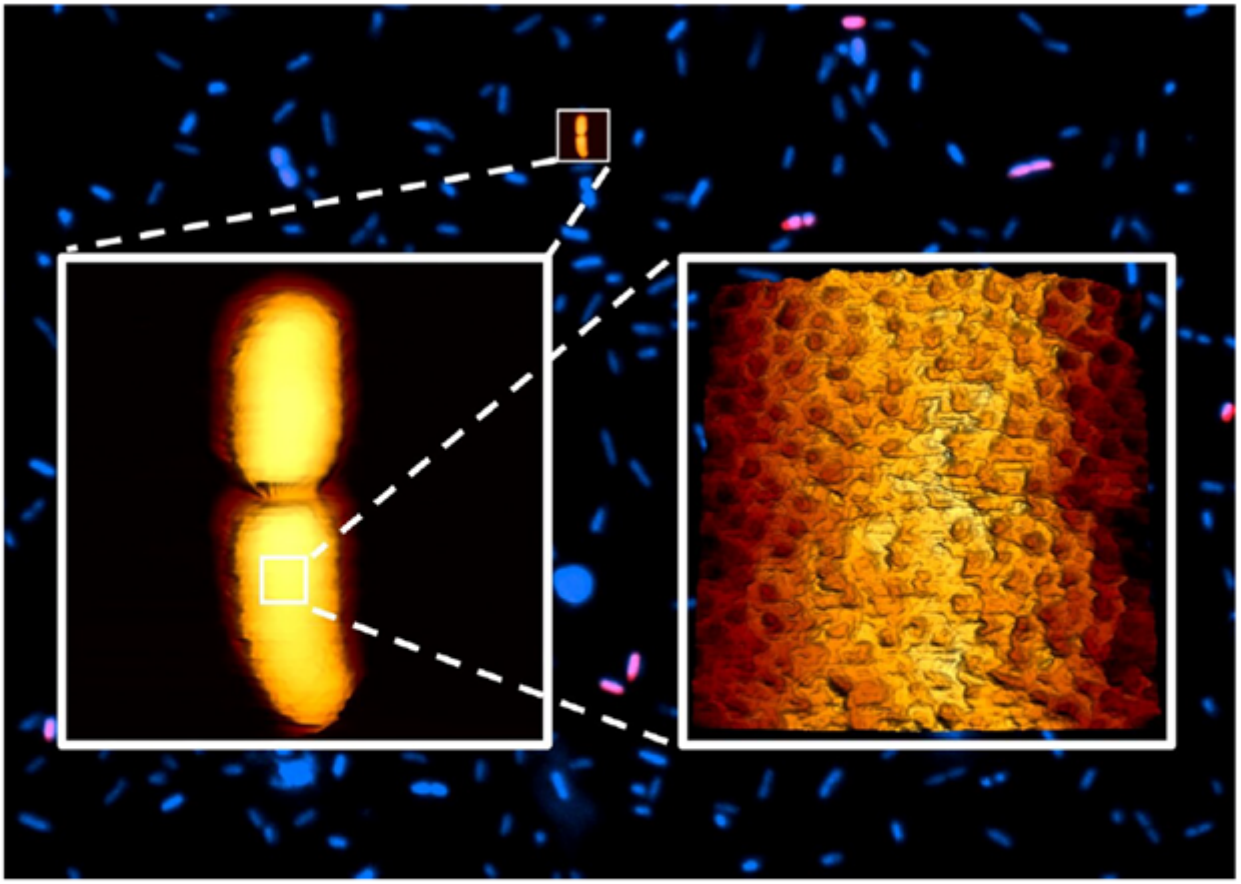

Correlative Microscopy of MG1655 bacterial species. Confocal laser scanning microscopy was used to localize living bacteria (Hoechst 33342, blue), while high-resolution fast AFM Imaging reveals the pore structure of the *E.coli* surface. NestedScanner AFM topography images acquired at 1 Hz line rate (overview) and 5 Hz line rate (zoom). XYZ ranges of the AFM regions are 4 µm x 4 µm x 1.4 µm (overview) and 200 nm x 200 nm x 15 nm (zoom).

Keywords:

AFM, Correlative Microscopy, Bacterial Imaging

169

Correlative analytical scanning electron microscopy reveals periprosthetic tissue response to nanoparticles and wear debris

Dr Louise Hughes[1], Pedro Machado[1], Joshua Lea[1], Zhidao Xia[2]
[1]Oxford Instruments NanoAnalysis, High Wycombe, UK, [2]Swansea University, Swansea, UK

Poster Group 2

Background
One of the leading factors in aseptic loosening, osteolysis, and subsequent failure of implants used for total joint replacement is the production of wear debris and the associated reaction in periprosthetic tissue [1]. Nanoscale wear particles (0.2-0.8µm) are a critical component in the activation of macrophages and inflammatory response [2]. Particle composition, identified using electron microscopy and energy dispersive x-ray spectroscopy (EDS), can determine their site of origin [3] and is a critical factor in macrophage cytotoxicity and the activation of pro-inflammatory cytokines [4]. However, EDS can only provide part of the information required to understand the molecular interactions between patient tissue and wear debris. Organic/inorganic molecules and their interactions are not detected by EDS alone.
Methods and aims
Here we present a correlative study incorporating a fast compositional imaging method for rapid identification of regions of interest (backscattered electron x-ray, BEX, imaging) across large tissue areas, combined with higher resolution EDS and Raman spectroscopy. Samples were prepared following methods presented by Xia et al. [3] with modification for scanning electron microscope (SEM). The uncoated resin-embedded tissue samples were imaged in a Zeiss Gemini460 SEM in variable pressure mode at 10kV using a Unity BEX imaging detector combined with an Ultim Max 100 EDS detector, followed by analysis with RISE (Raman Imaging Scanning Electron). RISE imaging was conducted using a 785 nm laser, tuned to 25 mW using the TruePower module. The multimodal imaging datasets were colocalised and overlayed using the Relate software package (version 9.3.10333).
Results and conclusions
We investigated the ultrastructure, chemical and elemental properties of tissue interacting different wear particles. We observed particles of titanium accumulated into large clusters (50 to 500µm) surrounded by tissue that had distinct density difference. High density areas of the tissue were characterised by an elevated weight percentage (wt%) of calcium (Ca) and phosphorus (P) (Figure 1 BEX). RISE analysis of the same region shows spectra indicating two phosphate populations: one spectrum was characteristic of hydroxyapatite, the second was bound to tissue stained with lead citrate with the presence of lead confirmed using both Raman spectroscopy and EDS. A third spectrum peak in the carboxylate region, overlays with the low-density tissue observed by BEX (Figure 1 RISE, RISE spectrum, BEX + RISE overlay). Similar results were observed in samples containing much smaller (<0.8µm) cobalt nanoparticles.
The multimodal and correlative approach combines the speed of BEX screening with high-resolution characterisation (EDS and RISE) of tissue reactions to nanoscale wear particles. The proposed correlative workflow can generate detailed structural and molecular data for studying the effects of metal nanoparticles from implants and may provide a fast screening technique to facilitate diagnostic analysis of pathological features in the future, in particular the molecular mechanism that triggers host allergic and inflammatory response to orthopaedic implants.
Fig 1. Overlayed BEX and RISE images show 3 distinct tissue phases characterised by different electron density (BEX), chemical (RISE, RISE spectrum) and elemental compositions (BEX, BEX+RISE overlay). BEX images display Uranium (U) and Lead (Pb) in cyan, Titanium (Ti) in yellow, Calcium (Ca)

in pink and Phosphorous (P) in blue, electron image in greyscale. RISE images and spectra: Hydroxyapatite in red, resin substrate in blue, metal bound Phosphate in green.

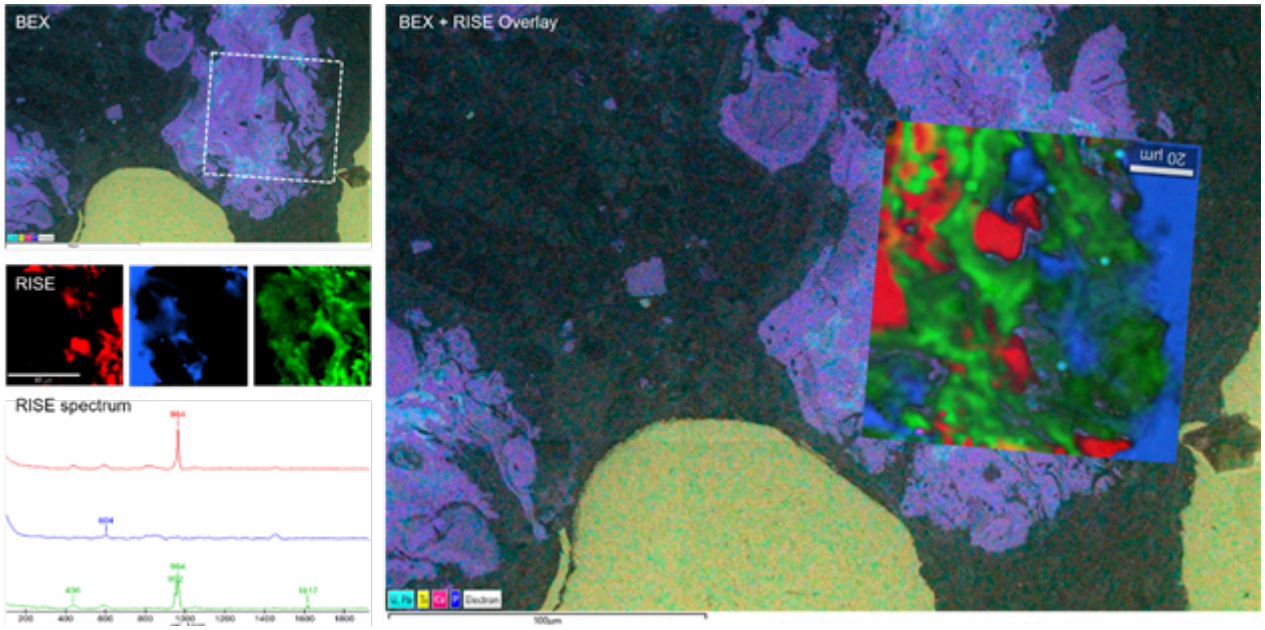

Keywords:

Correlative, EDS, Raman, BEX, SEM

Reference:

[1] National Joint Registry. Vol 2020. National Joint Registry; 2020.
[2] Ingham E, Fisher J. Biomaterials. 2005;26(11):1271-1286
[3] Xia, Z., et al., 2017. Nanomedicine: Nanotechnology, Biology and Medicine, 13(3), pp.1205-1217.
[4] Liu, Z., et al., 2023. Journal of Orthopaedic Translation, 38, pp.203-212.

178

Combining SIMS elemental mapping with FIB-based imaging for multimodal analysis of biological specimen

Dr. Antje Biesemeier[1], Mr. Olivier de Castro[1], Miss Tatjana Taubitz[1,2], Miss Zahraa Berro[1,3], Mr Jean-Nicolas Audinot[1], Mr Tom Wirtz[1]
[1]Advanced Instrumentation for Nano-Analytics, Materials Research and Technology Department, Luxembourg Institute of Science and Technology, Belvaux, Luxembourg, [2]Department of Structural Biochemistry, Max Planck Institute of Molecular Physiology, Dortmund, Germany, [3]Doctoral Programme in Systems and Molecular Biomedicine of the DSSE, University of Luxembourg, Belval Esch-sur-Alzette, Luxembourg

Poster Group 2

Background: The generation of chemical maps of sub-cellular structures in biological samples is one important tool to identify and localize accumulating ingested particles, drugs or metal tagged biomarkers. By correlating this chemical information obtained by spectroscopical methods like x-ray spectroscopy, etc. to an ultrastructural image obtained by light or electron microscopy the underlying physiological processes can be investigated. However, the better the lateral resolution of the chemical mapping, the lower the signal detected per voxel, oftentimes leading to inaccessibility of certain markers for chemical imaging in cells and tissues. In this regards, secondary ion mass spectrometry (SIMS) is a powerful technique for analyzing surfaces at high spatial resolution, owing to its ability to detect all elements from H to U and to differentiate between isotopes, its excellent sensitivity and its high dynamic range. Our group focuses on the development of multimodal imaging platforms giving access to correlative investigation approaches by directly linking SIMS data with data obtained by other analytical (such as Energy-Dispersive X-Ray Spectroscopy) or imaging techniques on the same instrument (e.g. secondary electrons (SE), back-scattered electrons (BSE) or images of the transmitted ion or electron beam (STIM, STEM)). The possible combinations are dependent on the sources and detectors available on these platforms.
Methods: Currently, several focused ion beam platforms with or without an additional electron column are available and are equipped with at least a secondary electron detector and LIST's magnetic sector SIMS system (FIB-SIMS with < 15 nm spatial resolution). These instruments use various primary ion beam species, such as Ga [1], He / Ne [2-3], Cs [4] as well as Si / Au / Li / Bi [5]. Our magnetic sector SIMS system is equipped with a continuous focal plane detector technology allowing parallel detection of all masses for each single pixel in the scanned region of interest. One instrument is also equipped for imaging the transmitted beam information and can be operated at RT and under cryogenic conditions facilitating the analysis of beam sensitive samples and frozen samples.
Results: A number of examples from different application fields (nanotoxicology, environmental pollution, water organisms etc.) will be presented.
Conclusion: The performance of the different instruments will be discussed with a focus on new developments, different SIMS acquisition modes (mass spectra, depth profiling, 2D and 3D chemical imaging) and their applicability for biological samples including frozen-hydrated specimen.

Keywords:

focused-ion-beam-microscopy, SIMS, correlative microscopy, cryoanalysis

Reference:

[1] Anal. Chem 94 (2022) 10754
[2] Rep. Prog. Phys. 84 (2021) 105901
[3] Anal. Chem. 93 (2021) 14417–14424

[4] Microscopy Microanalysis 27_S1 (2021) 24–25
[5] Microscopy Microanalysis 29_S1 (2023) 536–537

Funding information: This work received funding from the EUHorizon 2020 RIA Programme (GA no. 720964) and the FNR Luxembourg (INTER/DFG/19/13992454, CORE C21/BM/15754743).

402

Thapsigargin induces non-apoptotic programmed cell death in RBL-1 cells

Dr. Philip Steiner[1], Mr. Hubert Kerschbaum[2], Mrs. Ancuela Andosch[1,2], Mr. Korollus Melek[3], Mrs. Susanna Zierler[1,4]
[1]Institute of Pharmacology, Johannes Kepler University, Linz, Austria, [2]Department of Biosciences and Medical Biology, Paris Lodron University, , Austria, [3]Institute of Biochemistry and Molecular Medicine, University Bern, , Switzerland, [4]Walther Straub Institute of Pharmacology, Ludwig Maximilians University, Munich, Germany

Poster Group 2

Background and aims:
Thapsigargin (TG) is a potent sarco/endoplasmic reticulum (ER) Ca2+-ATPase (SERCA) inhibitor and, accordingly, elevates intracellular Ca2+ levels. Recent studies demonstrate that TG induces cell death in a variety of cancer cells. While it is assumed that TG triggers cell death by apoptosis, our cytological studies on rat basophilic leukemia cells (RBL-1) indicate a non-apoptotic mode of cell death.
Methods:
Since the ultrastructural hallmarks of TG-induced cell death are only sparsely described, we studied the morphological consequences of TG exposure in RBL-1 cells using 2D transmission electron microscopy (TEM) and 3D TEM tomography in correlation with laser scanning microscopy (LSM). To visualize and quantify the effects on different organelles, live-cell fluorescence markers such as ER-tracker, HOECHST, endocytosis-tracker and MitoTracker were used.
Results:
TG-exposed RBL-1 cells showed prominent ballooning of the perinuclear space, vacuolization, increased vesicle formation, mitochondrial enlargement and degradation as well as ER- swelling and anomalies. In particular, the TEM data failed to show apoptotic hallmarks such as nuclear fragmentation or the formation of apoptotic bodies in TG-exposed RBL-1 cells.
Conclusion:
Contrary to the prevailing theory that TG triggers apoptosis, our results suggest a non-apoptotic programmed cell death. Moreover, numerous non-apoptotic morphological hallmarks were found, which are reminiscent of autosis and paraptosis. Thus, while TG represents a potential tumor therapeutic agent, the underlying mechanisms of cell death are still ambiguous and might differ in distinct cell types.

Keywords:

apoptosis, autosis, paraptosis, thapsigargin, cancer

450

Evaluation of Conventional Adherent Cell Enumeration Methodologies alongside Image-Enhanced Flow Cytometry

Dr Matthew Bourn[1], Mrs Lauren Daly[1], Mr Scott Gregory[1], Mrs Jeanne Rivera[1]
[1]National Measurement Laboratory at LGC Ltd, Leeds, UK

Poster Group 2

Background incl. aims
Enumeration and characterisation of cell populations are vital processes in both clinical and industrial laboratories. Accurate, reproducible counts of viable and apoptotic cells are crucial to many biological assays and require the development of robust experimental protocols. Currently, interlaboratory comparability between cell measurements is limited due to the lack of alignment in cell analysis techniques and methodologies. In general, the enumeration of adherent cells poses a greater metrological challenge than suspension cells, due to morphological complexity and diversity these cells can present. The impact of cellular morphology and growth characteristics on cell counting is yet to be fully investigated for many conventional enumeration techniques. The use of DNA and membrane stains allowed for quantification of cell confluency as a function of cell count using microscopy, demonstrating the impact of cell type on limits of quantification and linearity. Overall, this study evaluated the efficacy of three common enumeration techniques: haemocytometry, microscopy and flow cytometry using five distinct adherent cell types. Finally, a novel counting technique, which uses combined brightfield imaging flow cytometry, was investigated as a means of overcoming the current limitations associated with conventional flow cytometry.

Methods
Five adherent cell types; MCF-7, HeLa, MRC-5, HUVEC, and CHO were selected to cover a range of morphologies and disease states. Cells were seeded at commonly used concentrations, recommended by the ATCC. Cells were analysed forty-eight hours after seeding, using six separate instruments across three different counting techniques: haemocytometry (automated Countess and manual), microscopy (confocal and widefield), and flow cytometry (Attune CytPix and Beckmann Coulter CytoFlex). Cells for haemocytometry and flow cytometry were detached for counting using TrypLE. Cells for microscopy were fixed using 4 % paraformaldehyde, then DNA and membranes stained using Hoechst 33342 (2 µg/ml) and Wheat Germ Agglutin 594 (2.5 µg/ml) respectively. Imaging was performed using a Zeiss LSM 880 confocal or a EVOS FL 2 Auto widefield microscope. Automated image analysis of nuclei counts, and membrane area was performed using CellProfiler 4.2.1.

Results
Cell counts measured using hemocytometry demonstrated that this technique is least impacted by cellular morphology and growth characteristics. Low sampling volumes and user bias are the primary sources of counting variations which result in a relatively high limit of detection when compared to other techniques. The efficacy of microscopy-based counting was the most influenced by cellular morphology. Cells which displayed densely populated growth characteristics, such as CHO and HeLa, proved challenging in the identification and segmentation of single cell nuclei. These limitations resulted in a loss of linearity in cell count v confluency plots, which showed cell counts continuing to rise despite having a 100 % confluency. Both conventional flow cytometers consistently underestimated cell counts when compared to the other four techniques. This was primarily due to the presence of cell aggregates in the sample which were incorrectly counted as single cell events and was not resolved following single gating approach of scatter height against width. In particular, cells displaying clustered growth morphologies, such as MCF-7, were found to produce the lowest

cell counts in flow cytometry. Using the Attune CytPix brightfield imaging and analysis capabilities, cell aggregates could be identified and the number of cells in each aggregate determined. Image enhanced cell counts (CytPix En.) displayed values significantly more in-line with alternative techniques, demonstrating the efficacy of this novel counting methodology (graphic).

Conclusion

Results throughout this cell counting study demonstrated the impact of cell morphology and growth characteristics on countability. Several key factors have been highlighted which must be considered when aiming to develop robust cell counting methodologies and standards. Microscopy has been shown to be a useful tool for cell counting, however, this study notes that its limit of linearity and quantification is dictated by cell type. The combined use of flow cytometry and imaging for cell counting presents a quantitative method of determining cell count without the use of reference materials. This method overcomes the limitations of both microscopy and flow cytometry, in particular, removing the uncertainties associated with user-based single-cell gating strategies.

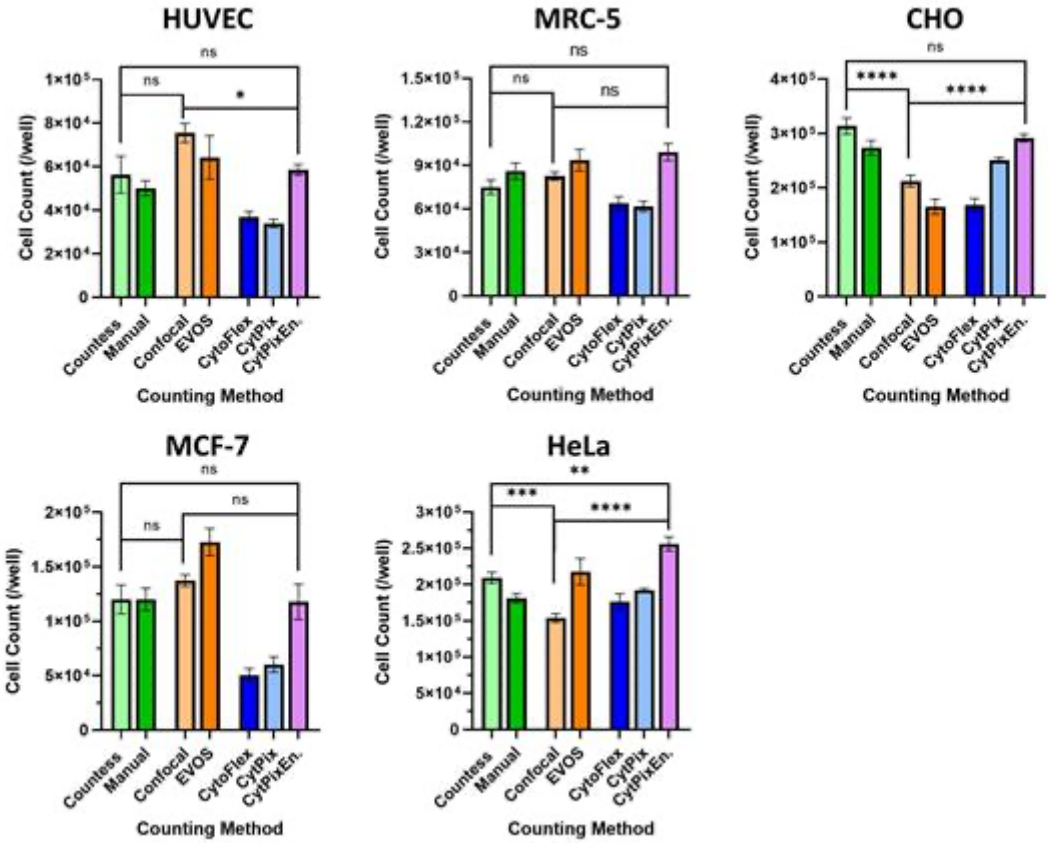

Keywords:

Cell-counting, Imaging Flow Cytometry, Microscopy

Reference:

Sarkar, S., Pierce, L., Lin-Gibson, S., & Lund, S. P. (2019). Standards Landscape in Cell Counting: Implications for Cell & Gene Therapy. Cell and Gene Therapy Insights, 5(1), 117–131. https://doi.org/10.18609/cgti.2019.016

Faruqui, N., Kummrow, A., Fu, B., Divieto, C., Rojas, F., Kisulu, F., Cavalcante, J. J. V., Wang, J., Campbell, J., Martins, J. L., Choi, J. H., Sassi, M. P., Zucco, M., Vonsky, M., Vessillier, S., Zou, S., Fujii, S.

I., & Ryadnov, M. G. (2020). Cellular Metrology: Scoping for a Value Proposition in Extra- and Intracellular Measurements. In Frontiers in Bioengineering and Biotechnology (Vol. 7). Frontiers Media S.A. https://doi.org/10.3389/fbioe.2019.00456

Runov, A. L., Shevchenko, N. N., Goryachaya, T. S., Kurchakova, E. v., & Vonsky, M. S. (2022). Metrology of cellular analysis: Problems and solutions. Journal of Physics: Conference Series, 2192(1). https://doi.org/10.1088/1742-6596/2192/1/012012

556

The organization of organic/biominerals in the nanostructured 3D photonic crystals in insects' scales

Dr. Yin Chang[1], Dr. Hsiang-Han Tseng[2], Dr. Luca Bertinetti[1], Dr. Michaela Wilsch-Bräuninger[3], Prof. Yael Politi[1]
[1]B CUBE - Center for Molecular Bioengineering, Technische Universität Dresden, Dresden, Germany, [2]Thermo Fisher Scientific, 1, The Felbridge Centre, Imberhorne Lane, East Grinstead, West Sussex, UK, [3]Max Planck Institute of Molecular Cell Biology and Genetics, , Germany

Poster Group 2

Background incl. aims
The colorful patterns displayed by longhorn beetles Doliops similis (Cerambycidae: Laminae) are formed by opalescent photonic structures confined within their cuticular scales [1]. The layers of packed nanospheres produce opalescent green colour. The morphogenesis of the nanoparticles in each scale and their self-assembly into opal-structures are unknown. We wish to employ correlative and multimodal imaging in our workflow that combines FIB/SEM volume imaging with super resolution microscopy of intact scales in order to monitoring the organic molecules distribution in the scale and in the photonic crystals.

Methods
Focus Ion Beam Scanning Electron Microscope (FIBSEM) was used to collect sequential images with voxel size of 5 nm. 3D model of 3580x 840x 270 voxels FIB-SEM stack at 5 nm resolution. Data were segmented by binarization after denoising (n2v [2]) and oriented domains were extracted using customized pipeline derived from the open source bmmltools [3].
With Fourier-transform Infrared Spectroscopy (FTIR), Small/Wide Angle X-ray Scattering and X-ray Fluorescence (SAXS/WAXS/XRF), we are able to measure the compositions in the scale, in the skin of the scale, and in the photonic crystals. Complemented with Depth-profiling Time-of-Flight SIMS (TOF-SIMS), X-ray Photoelectron Spectroscopy (XPS, NEXA G2, Thermofisher Scientific), we can understand the distribution and binding states of components with high resolution (<10 nm) in axial direction of an intact scale (60 x 40 x 5 um).

Results
We demonstrate that these needle-like scales contain a core-shell structure with a thin cuticular skin and an inner core of agglutinated amorphous calcium phosphate nanospheres (ACP, diameter of 160 nm). The spheres assemble into hexagonally close-packed layers along the surface normal of the scale, producing hence a uniform and intense green reflection colour. We successfully located the chitin fibers in the skin by applying chitin-binding proteins on sections of scales and visualized the distribution of chitin/proteins in the skin of the scales [4].

Conclusion
Our results show the D.similis longhorn beetles are able to produce highly-orderred arranged ACP nanoparticles within every micrometer-sized scale. From our preliminary results of IR, TOFSIMS, XPS, and super resolution microscope (Zeiss Elyra Sim2), we observed the co-existence of short chain lipids with the ACP nanoparticles in the core of the scale. Such observation seems an agreement with one of the hypotheses in biomineralization that the arrangement of chitin and (lipo-)protein at the interface of the cuticular shell and mineraloid core mediates the packing of the nanospheres [5]. To address this hypothesis, we wish to employ tissue clearing methods with correlative imaging to observe the networks and conformations of organic molecules in the intact scale and their association with the ACP opal photonic crystals.

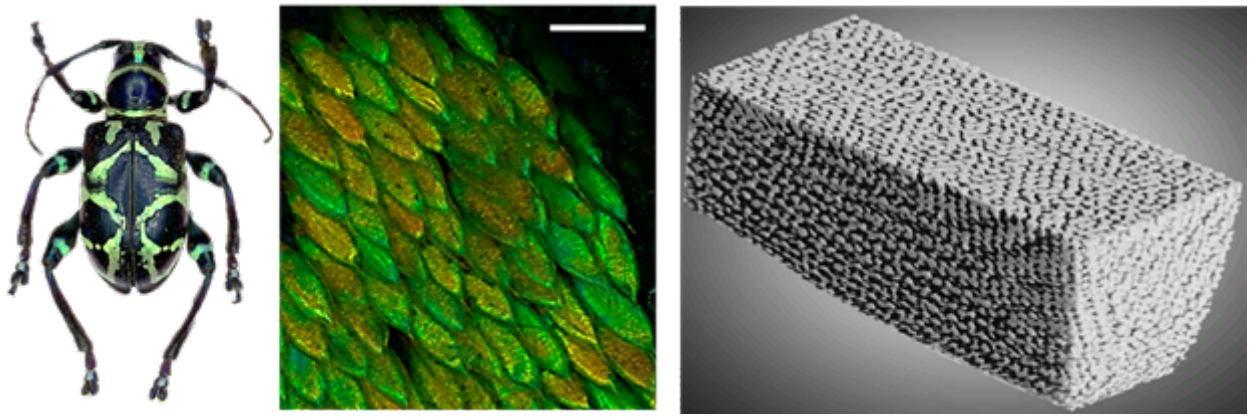

Keywords:

photonic crystals, biomineralization, volume imaging

Reference:

1. Chang Y. Chapter 6 Structural designs in the mimicry pair, In Multi-Functional nano-structures in Nature: from optics to mechanics. Diss. University of Cambridge, 2020; pp. 130-152
2. Krull A, Buchholz T and Jug F, "Noise2Void - Learning Denoising From Single Noisy Images," in 2019 IEEE/CVF Conference on Computer Vision and Pattern Recognition (CVPR), Long Beach, CA, USA, 2019 pp. 2124-2132.
3. bmmltools (https://bmmltools.readthedocs.io/en/latest/index.html)
4. Weiss Ingrid M., Schönitzer V, Eichner N and Sumper M, The chitin synthase involved in marine bivalve mollusk shell formation contains a myosin domain, FEBS Letters 2006, 580, doi: 10.1016/j.febslet.2006.02.044
5. Weiner S. Organization of organic matrix components in mineralized tissues, American zoologist 1984, 24; pp. 945-951

713

Correlative cryo soft x-ray tomography and fluorescent microscopy of biological samples in the laboratory

Mr Kenneth Fahy[1], Dr. Sergey Kapishnikov[1], Dr. Paul Sheridan[1], Mr. William Fyans[1], Dr. Fergal O'Reilly[1,2,3], Mr. Tony McEnroe[1]
[1]SiriusXT, Dublin, Ireland, [2]UCD School of Physics, Dublin 4, Ireland , [3]UCD School of Biology and Environmental Science, Dublin 4, Ireland

Poster Group 2

Background incl. aims
Soft x-ray tomography (SXT) uses low energy x-rays to image frozen-hydrated biological specimens such as entire mammalian cells or thick tissue slabs with a few tens of nanometers of spatial resolution. The technique takes advantage of the biological water window whereby water is relatively transparent to x-rays from 284 to 543 eV (2.34 to 4.4 nm) but carbon-based organelles are absorbing. This native contrast imaging allows high resolution imaging of bulk specimens with minimal sample preparation. While SXT has traditionally been confined to synchrotrons the recent development of a laboratory scale SXT microscope opens the possibility of integrating this novel technique into light and electron imaging workflows. The SXT microscope features an integrated light microscope for overview imaging and fluorescence targeting, allows for swift acquisition of 2D and 3D x-ray images covering extensive areas on the specimen, and enables efficient and rapid identification of cells of interest. The utility of the microscope is currently being demonstrated through 2 EU-funded consortia (https://cocid.eu/ and https://clexm.eu/). Recent case studies have included correlative imaging of whole, virus infected cells treated with anti-viral drugs; imaging the 3D distribution of therapeutic-laden nanoparticles in whole cells; and the development of correlative workflows for tissue imaging across scales. An alternative sample carrier in the form of a thin-walled glass capillary was also developed, further enhancing the novelty of the lab-based microscope.
Methods
Integrated cryo fluorescence was used to screen an entire EM grid for cell selection and correlation with SXT. Low magnification/large field of view 2D x-ray mosaics were then acquired over large areas of the grid before acquiring tilt series from ±60° on selected targets. Data from both modalities were then overlaid to provide the location of fluorescent proteins in the context of whole cell ultrastructure. For cells suspended in glass capillaries the tilt series was acquired over ±90°.
Results
Resulting cryo-SXT tomograms and fluorescent light images of cellular organelles and nanoparticles provide proof of concept for the lab-based microscope and associated workflows.
Conclusion.
Workflows of correlative light, electron and soft x-ray microscopy combines the strengths of each modality. The recent availability of a compact soft x-ray microscope will accelerate the development of novel workflows and biological imaging applications that can benefit from this technique. We will present our microscope workflows and application data.

Keywords:

Soft x-ray tomography, fluorescent microscopy

Reference:

Acknowledgement

We acknowledge funding from the European Union's Horizon 2020 Research and Innovation programme (No. 101120151, project CLEXM and No. 101017116, project CoCID) as well as the Irish Research Council (No. EBPPG-2020-278).

809

Inflammatory mechanism in Diabetes – Ultrastructural investigations of endocrine pancreas using correlative electron microscopy (STEM)

Dr. Dagmar Kolb[1,2], Bsc. Sumayya Böhm[1], Kerstin Hingerl[1], Prof. Thomas Pieber[3,4], Msc. Barbara Ehall[3,4], Bsc. Dominique Pernitsch[1], DI Lea Bogensperger[5]
[1]Core Facility Ultrastructure Analysis - Center for Medical Research, Graz, AUSTRIA, [2]Gottfried Schatz Research Center, Division of Cell Biology, Histology and Embryology, Graz, AUSTRIA , [3]Division of Endocrinology and Diabetology, Medical University of Graz, , , [4]The Center for Biomarker Research in Medicine GmbH, , , [5]Institute of Computer Graphics and Vision, Graz University of Technology, ,

Poster Group 2

Patients suffering with type 1 diabetes show a major reduction of beta cells within their endocrine pancreas. To gain deeper insights into mechanisms of beta cells, correlative electron microscopy was the method of choice to understand the ultrastructure of insulin producing beta cells. The first step of this workflow was scanning electron microscopy employing the STEM (scanning transmission electron microscopy) detector. STEM images were generated with the benefit of great overviews on the one hand and giving information on cell interaction and arrangement within the entire organ at high resolution on the other hand. For an even more detailed investigation a suitable region of interest (ROI) in the pancreatic islets was preselected on STEM images. The sample was subsequently observed in the transmission
electron microscope (TEM) which was possible without any further processing. To gather more information on the respective healthy and diabetic phenotypes, we used a deep learning-based approach to achieve high classification accuracy when discriminating between healthy and NOD samples of beta cells. We further explored the link between the number of granules in a sample and the healthy/NOD class it belongs to. Applying this insight to train neural networks that jointly learn both classification and counting tasks or rely on transfer learning strategies, performance on classification is improved. The additional counting tasks allow for a more robust representation, which is especially useful since only limited data are available. The findings strongly support the underlying hypothesis that early onset diabetes leads to a reduction in insulin-containing granules. Nevertheless, classification on its own already delivers strong results: There are additional factors other than the number of granules that play a major role in the decision process, such as changed appearances in the granules themselves or the surrounding tissue.

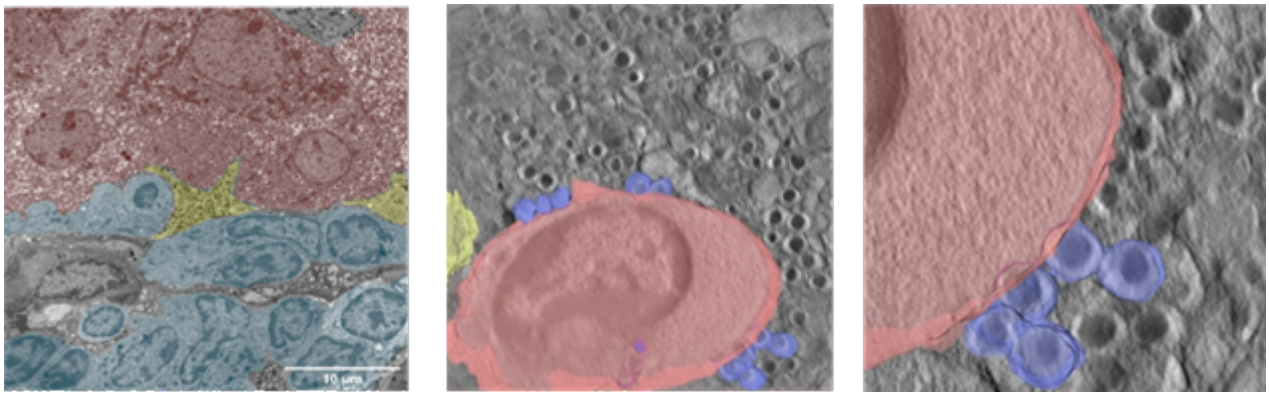

Keywords:

Scanning transmission electron microscopy; diabetes

Reference:

Lea Bogensperger, Erich Kobler, Dominique Pernitsch, Petra Kotzbeck, Thomas R. Pieber, Thomas Pock, and Dagmar Kolb. “A Joint Alignment and Reconstruction Algorithm for Electron Tomogra-phy to Visualize In-Depth Cell-to-Cell Interactions.” Histochemistry and Cell Biology, 2022.

826

Three-dimensional, correlative electron microscopy and immuno-labelling revealed new principles of the Golgi complex functioning

Prof. M.D.; PhD.; DcS. Alexander Mironov[1], MD, PhD, DcS Galina Beznoussenko[1]
[1]IFOM ETS—The AIRC Institute of Molecular Oncology, Milan, Italy

Poster Group 2

Goal. The Golgi complex (GC) is one of the main organelles of the cell, it has a complex organization and provides transport of proteins and lipids, as well as their glycosylation. It was necessary to understand the principles of the GC operation.
Methods. The use of three-dimensional electron microscopy (EM), immune EM, and correlative light EM made it possible to abandon the use of the old radigma explaining Golgi function and provide the new one [1, 2].
Results. We have shown that membrane spherical vesicles in the area of endoplasmic reticulum (ER) exits sites are produced mostly with the help of a COPI/ARF machine. There are no completely isolated carriers between the ER and GC. COPI-dependent Golgi vesicles contain a sharply reduced content of retrograde and anterograde cargoes. At the same time, during their transport through the GC, the concentration of soluble, membrane and mega-cargoes increases, which cannot be explained using the maturation model [3, 4].
The role of cisternal perforations for intra-Golgi transport is shown [5].
It was found that the GC may be in a state of rest or transport. The non-transporting GC does not have a cis-most and trans-most cisternae attached to the poles of the medial GC. The beginning of transport leads to their attachment to the stack of medial cisternae in a GM130 and G97 dependent manner, respectively.
The size of the exit site from the GC depends on the amount of cargo being transported [3,4]. With the synchronous movement of a large number of cargo, the exit is carried out from the last two medial cisternae and TMC. When transporting a small amount of cargo, the last medial cisterna and TMC function as the Golgi exit site.
Membrane fusion is important for both moving through and exiting the GC. Post-Golgi carriers ferrying cargoes to the baso-lateral plasma membrane are not completely isolated and always pass through endosomes to change the set of their SNAREs.
The mapping of the main protein machines involved in intracellular transport in various compartments and during various functional states, as well as their changes in different phases of the cell cycle, are presented [2, 5].
Conclusion. The intracellular transport model based on the kiss-and-ran mechanism most fully corresponds to the data obtained.

Keywords:

Golgi; Electron microscopy, Transport, Correlative

Reference:

1. Mironov AA, Beznoussenko GV. Algorithm for Modern Electron Microscopic Examination of the Golgi Complex. Methods Mol Biol. 2023;2557:161-209. doi: 10.1007/978-1-0716-2639-9_12.
2. Mironov, A,A.; Beznoussenko, G.V. Models of Intracellular Transport: Pros and Cons. Front. Cell Dev. Biol. 2019, 7, 146. doi: 10.3389/fcell.2019.00146.
3. Mironov AA, Beznoussenko GV. The Regulated Secretion and Models of Intracellular Transport: The Goblet Cell as an Example. Int J Mol Sci. 2023 May 31;24(11):9560. doi: 10.3390/ijms24119560.

4. Sesorova IS, Karelina NR, Kazakova TE, Parashuraman S, Zdorikova MA, Dimov ID, Seliverstova EV, Beznoussenko GV, Mironov AA. 2020. Structure of the enterocyte transcytosis compartments during lipid absorption. Histochem Cell Biol. 2020 Jun;153(6):413-429. doi: 10.1007/s00418-020-01851-3
5. Beznoussenko, G.V.; Kweon, H.S.; Sesorova, I.S.; Mironov, A.A. Comparison of the Cisterna Maturation-Progression Model with the Kiss-and-Run Model of Intra-Golgi Transport: Role of Cisternal Pores and Cargo Domains. Int J Mol Sci. 2022, 23, 3590. doi: 10.3390/ijms23073590.

869

Combination of TEM, LM and micro-CT to image insects: the perspective of crop protection strategies

Nada Žnidaršič[1], Urban Bogataj[1], Polona Mrak[1], Katja Kunčič[1], Miloš Vittori[1], Primož Žigon[2], Jaka Razinger[2], Jerica Sabotič[3]
[1]University of Ljubljana, Biotechnical Faculty, Department of Biology, Ljubljana, Slovenia, [2]Agricultural Institute of Slovenia, Plant Protection Department, Ljubljana, Slovenia, [3]Jožef Stefan Institute, Department of Biotechnology, Ljubljana, Slovenia

Poster Group 2

Background

Invasive insects, in addition to several already established species, are a serious threat to crop production and an important hazard as vectors of pathogens of severe diseases. This is an increasing problem due to trans-continental trade, travel and climate change. Therefore, new strategies for crop protection and new approaches to minimize the adverse effects of pathogen spread are needed. A better understanding of insect functional ultrastructure during animal development and under stress conditions is crucial to facilitate formulation of new innovative solutions. Microscopic analyses enable comprehensive characterization of the structure of insect organs and localization of selected molecules at different scales, and in combination with biochemical analyses that unravel selected aspects at the molecular level, constitute a toolbox for the integration of structure and function and for an in-depth evaluation of the effects of xenobiotics. The first aim of our study was to establish a procedure in which micro-computed tomography, light and transmission electron microscopy will be used in combination to image insect digestive system in larvae and adults, spanning the range from molecular resolution to imaging of the whole organisms. Our second aim was to apply the method to characterize the midgut of two insect species that are important from the perspective of crop protection, spotted wing drosophila (Drosophila suzukii) and Colorado potato beetle (Leptinotarsa decemlineata).

Methods

The insect gut is positioned at the interface between the external and internal environment and it is a likely target of xenobiotics. As the midgut epithelium plays a central role in digestion, nutrient absorption and protection against toxins and pathogens, we have characterized the midgut functional ultrastructure in larvae and adults to get insight into changes during development and to evaluate the alterations of the gut epithelium due to exposure to selected xenobiotics - fungal lectins and protease inhibitors. Micro-CT imaging was performed on whole animals that were chemically fixed. Subsequent processing and segmentation of the micro-CT data was performed using Neoscan80 and Dragonfly software. Sections of the whole larvae or dissected gut samples were imaged by LM and TEM in different regions along the anterior-posterior axis, focused on the characterization of the luminal surface of the epithelium, the distribution of stem/progenitor cells and alterations of the epithelium architecture after exposure to selected xenobiotics.

Results and conclusions

The digestive system in insects consists of foregut, midgut and hindgut. The highly convoluted midgut is the longest part of the alimentary canal and occupies a large part of D. suzukii larva body volume (Figs. 1A, B). The midgut epithelium comprises several cell types (Fig. 1C), enterocytes bear numerous microvilli on the apical surface (Fig. 1D). Stem cells are abundant and appear as clusters of cells in the basal region of the epithelium (Fig. 1E). In the midgut of Colorado potato beetle larvae columnar enterocytes with dense apical microvilli prevail and numerous stem cells reside in clusters in the basal part of the gut epithelium. Stem cells do not form septate junctions with neighbouring cells,

while enterocytes display abundant intercellular junctions. Our current work is focused on the determination of the effects of entomotoxic fungal proteins on the digestive system by a combination of imaging methods and biochemical approaches to identify the target molecules and elucidate their mode of action.

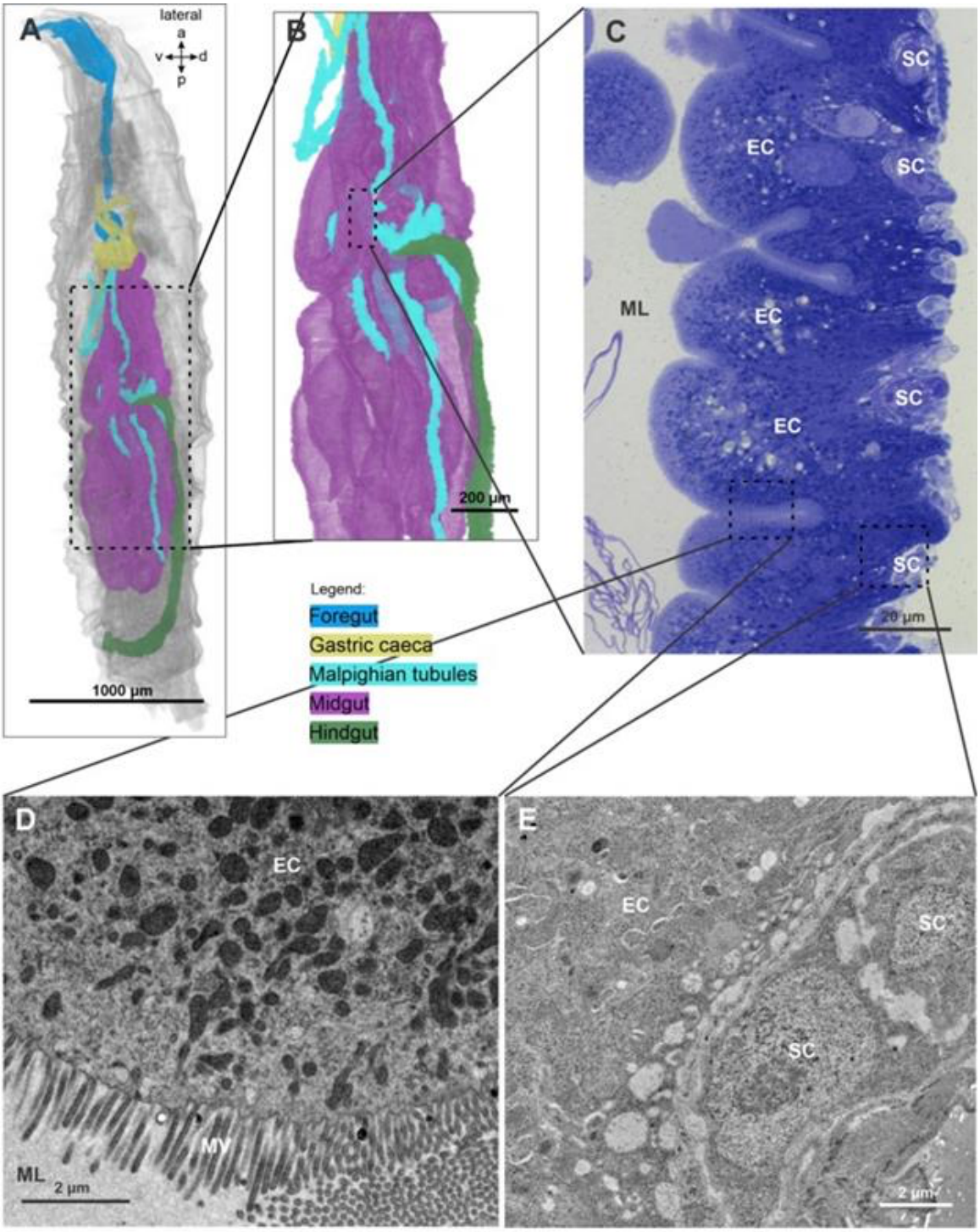

Figure 1: A, B) Micro-CT 3D reconstruction of the digestive system in *D. suzukii larva.* **C)** Histological structure of *D. suzukii* midgut epithelium and peritrophic matrix in the midgut lumen (ML). **D)** Electron micrograph of the apical surface of enterocyte (EC) with microvilli (MV). **E)** Electron micrograph of basally located midgut stem cells (SC).

Keywords:

Midgut, stem cells, insect larvae

895

Microvessel and mitochondria changes in a mouse model of Alzheimer's disease

DVM PhD Stine Hasselholt[1,2], Cagla Cömert[2,3], Jesper Just[2,4], Peter Bross[3], Jens Randel Nyengaard[1,5], Brian Hansen[2], Leif Østergaard[2]
[1]Core Centre for Molecular Morphology, Dept. of Clinical Medicine, Aarhus University, Aarhus, Denmark, [2]Center of Functionally Integrative Neuroscience, Dept. of Clinical Medicine, Aarhus University, Aarhus, Denmark, [3]Research Unit for Molecular Medicine (MMF), Dept. of Clinical Medicine, Aarhus University, Aarhus, Denmark, [4]Dept. of Molecular Medicine (MOMA), Dept. of Clinical Medicine, Aarhus University, Aarhus, Denmark, [5]Dept. of Pathology, Aarhus University Hospital, Aarhus, Denmark

Poster Group 2

Background and aim: Reduced oxygen availability is prevalent in several conditions affecting the brain including Alzheimer's disease [1, 2]. The mitochondria are main consumers of oxygen for ATP production, and the mitochondrial network adapts to changes in substrate availability and metabolic needs of the cell with dynamic shape transitions. Fusion of mitochondria enables transfer/sharing of organelle components, thereby improving energy conversion efficiency, and fission makes removal of damaged mitochondria possible. The cristae of the inner mitochondrial membrane, where oxidative phosphorylation takes place, are also remodelled in adaptation to energy substrate availability. The close relation between mitochondria morphology and function makes analyses of this organelle valuable in the search of an improved understanding of the subcellular effects of decreased tissue oxygenation in vivo. This is central in the elucidation of Alzheimer's disease pathogenesis and identification of novel therapeutic targets. We aim to investigate the effect of insufficient oxygen availability on the structure and function of mitochondria in a mouse model of Alzheimer's disease.
Methods: At the microscale, brains undergo MR scanning to examine the correlation between non-invasive detection of structural modelling and subsequent histological observations. Capillaries from the hippocampal strata oriens, -radiatum, and -lacunosum moleculare in CA1 are analysed using stereology to assess vascular changes. Based on these findings, a specific stratum is chosen for nanoscale analysis of mitochondria using vEM. The total volume and volume distribution of mitochondria are acquired, and crista related parameters evaluated in 3D applying our newly developed method [3]. Mitochondrial respiration is assessed with Seahorse assays on tissue punches and isolated mitochondria obtained from the hippocampus.
Results and Conclusion: Analyses are ongoing and hopefully results can be presented at EMC2024.

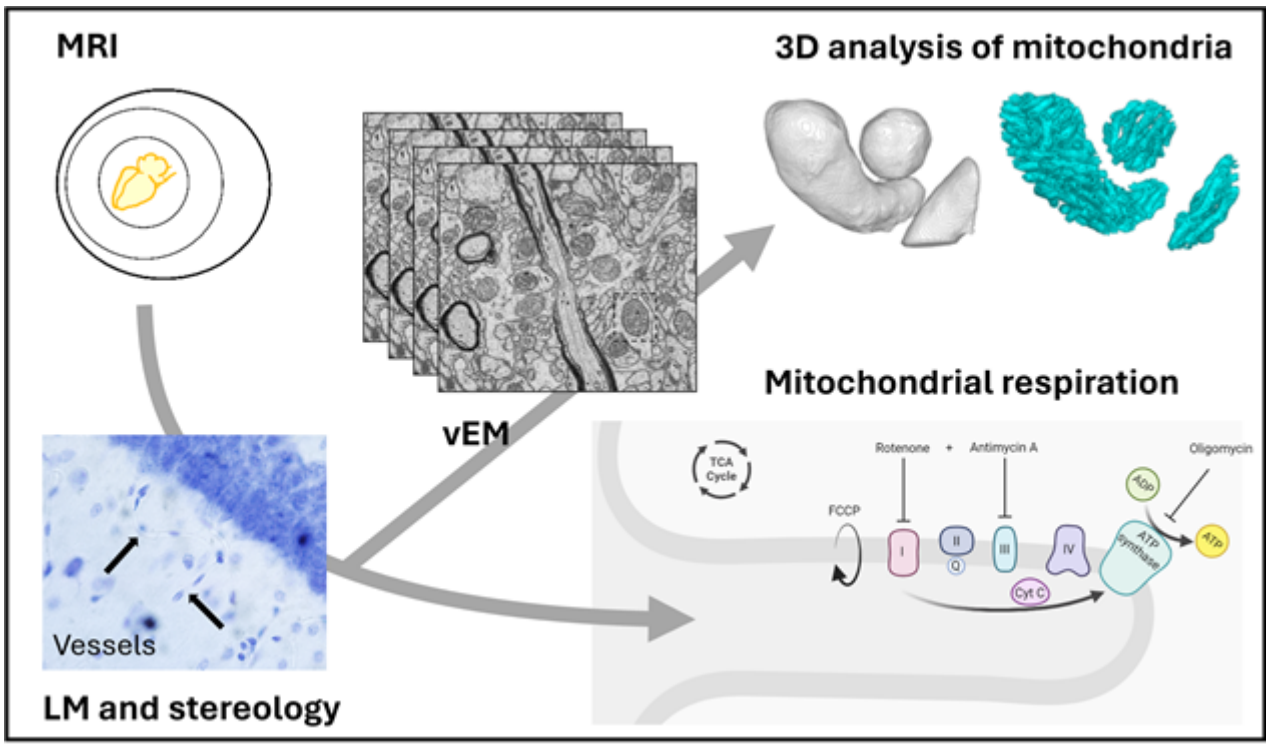

Keywords:

cross-scale microscopy, microvessels, mitochondria, Seahorse

Reference:

1. Nortley, R., et al., Amyloid beta oligomers constrict human capillaries in Alzheimer's disease via signaling to pericytes. Science, 2019. 365(6450): p. eaav9518.
2. Kisler, K., et al., Cerebral blood flow regulation and neurovascular dysfunction in Alzheimer disease. Nat Rev Neurosci, 2017. 18(7): p. 419-434.
3. Wang, C., et al., A semi-automatic method for extracting mitochondrial cristae characteristics from 3D focused ion beam scanning electron microscopy data. Commun Biol, 2024. 7(1): p. 377.

948

Human Tumor Microbiome Detection using Correlative Light and Electron Microscopy

Dr. Tali Dadosh[1], Dr. Smadar Levin-Zaidman[1], Dr. Deborah Nejman[2], Dr. Nancy Gavert[2], Prof. Ravid Straussman[2]
[1]Department of Chemical Research Support, Weizmann Institute of Science, Rehovot, Israel,
[2]Department of Molecular Cell Biology, Weizmann Institute of Science, Rehovot, Israel

Poster Group 2

In recent years, bacteria have shown to be present of human tumors, but their role and advantageous to the tumors or to the bacteria themselves is still mostly unclear. Characterization of the tumor microbiome is challenging because of its low biomass. In order to confirm the presence of bacteria in human tumors, various methodologies were conducted including immunohistochemistry by using antibodies against bacterial lipopolysaccharide and lipoteichoic acid to detect Gram-negative and Gram-positive bacteria, respectively. However verifying the presence of bacteria inside cancer cells is challenging, due to the small size of the bacteria and its sparsity in the tumor tissue. We used Correlative Light-Electron Microscopy (CLEM) that localize specific cellular components using fluorescence labeling and microscopy and visualize in high resolution details the cell ultrastructure by electron microscopy. Fluorescent labeling has been used to identify bacteria over a large area of interest in a sample, and particularly beneficial in samples exhibiting a sparse number of targets or events. In this work we were able to validate the presence of bacteria inside cancer cells of human breast tumor. Combined fluorescence staining of bacteria and transmission electron microscopy imaging of the same cells clearly demonstrated the intracellular localization of bacteria in tumors [1].

Keywords:

CLEM, Light and electron microscopy

Reference:

D. Nejman, I. Livyatan, G. Fuks, et al., The human tumor microbiome is composed of tumor type-specific intracellular bacteria, Science, 368 (6494) (2020), pp. 973-980

1095

Laboratory Soft X-ray Microscopy for Biomedical Applications

Aurélie Dehlinger[1,2], Dr. Christian Seim[1,2], Valentina Alberini[1,2], Dr. Holger Stiel[2,3], Dr. Antje Ludwig[4,5,6], Sarah Jung[1,2], Daniel Groetzsch[1,2], Vladimir Usatikov[1,2], Dr. Johannes Tuemmler[3], Prof. Dr. Birgit Kanngießer[1,2]
[1]Technische Universität Berlin, Institut für Optik und Atomare Physik, Berlin, Germany, [2]Berlin Laboratory for innovative X-ray technologies (BLiX), Berlin, Germany, [3]Max-Born-Institut (MBI) im Forschungsverbund Berlin e.V., Berlin, Germany, [4]Department of Cardiology, Angiology and Intensive Care Medicine, Deutsches Herzzentrum der Charité, Berlin, Germany, [5]Department of Cardiology, Angiology and Intensive Care Medicine, Charité - Universitätsmedizin Berlin, Corporate Member of Freie Universität Berlin and Humboldt-Universität zu Berlin, Berlin, Germany, [6]DZHK (German Centre for Cardiovascular Research), Partner Site Berlin, Berlin, Germany

Poster Group 2

Background incl. aims: Soft X-ray microscopy is a powerful tool for three-dimensional investigation of biological material [1]. The water window energy range between the absorption edges of carbon (284 eV) and oxygen (543 eV) provides a strong natural contrast for aqueous samples and offers the possibility for both a high resolution of a few tens of nanometer and a high penetration depth of up to 10 µm. Within the Collaborative Research Center 1340 (CRC) “Matrix in Vision” funded by the German Research Foundation, we use soft X-ray microscopy to investigate the role of the extracellular matrix (ECM) in diseased tissue, as the components and properties of the ECM play a major role in the regulation of cell and tissue function.
Methods: Alteration of the ECM plays a pivotal role in the progression of inflammatory diseases such as atherosclerosis. Understanding the underlying processes contributing to ECM alterations can aid in early detection during the initial stages of development. The ECM of cryofixed model cells (THP-1 cell line derived from an acute monocytic leukemia patient) has been studied with a laboratory soft X-ray microscope (L-TXM) located at the Berlin Laboratory for innovative X-ray Technologies (BLiX) at TU Berlin. A correlative workflow was developed by integrating a visible light microscope into the L-TXM setup [2], allowing a fast transition between the two modalities, and facilitating sample localization to accelerate 3D cell imaging. Additionally, various upgrades have been performed on the L-TXM setup to enhance stability and increase sample throughput in order to streamline the workflow and address the specific demands of the samples investigated within the CRC.
Results: The upgraded L-TXM at TU Berlin offers enhanced stability and increased sample throughput for biomedical research within the CRC, resulting in consistent imaging quality over extended acquisition times. Laboratory-based soft X-ray microscopy was able to resolve the THP-1’s glycocalyx – an intricate fragile extracellular structure. Nevertheless, different sample preparations resulted in different thicknesses and lengths of the glycocalyx’s interlocking meshy structure.
Conclusion: Laboratory soft X-ray microscopy provides unique flexibility and access to high resolution 3D imaging. Recent upgrades of the laboratory setup now enable a more streamlined workflow. The resulting higher sample throughput will help to establish suitable preparation techniques for various cell types for soft X-ray ECM research within the CRC. Combining results from X-ray based analytics with clinical diagnostics adapted for ECM research will help to better understand the role that the extracellular matrix plays in (inflammatory) diseases.

Keywords:

Soft X-ray Microscopy, Extracellular Matrix

Reference:

[1] Kördel, M. et al., (2020). Optica Vol. 7, issue 6, pp. 658-674
[2] Dehlinger, A. et al., (2020). Microscopy and Microanalysis Vol. 26, Issue 6, pp. 1124-1132

1205

Revealing foliar nanoparticle uptake dynamics: integrating nano-CT, confocal microscopy and LA-ICP-MS insights

Phd Student Andrea Pinna[1], PhD student Emil Visby Østergaard, PostDoc Noemie Thiebaut, Professor Rajmund Mokso, Professor Søren Husted
[1]University of Copenhagen, Copenhagen, Denmark

Poster Group 1

Revealing foliar nanoparticle uptake dynamics: integrating nano-CT, confocal microscopy and LA-ICP-MS insights
Andrea Pinna1, Emil Visby Østergaard2, Rajmund Mokso2, Noémie Thiébaut1, Søren Husted 1
1 University of Copenhagen, Copenhagen, DK, 2 Technical University of Denmark, Lyngby, DK
Background incl. aims
The agriculture sector calls for urgent action on novel strategies that can enhance fertilizers' efficiency in order to increase crop production while reducing its environmental footprint. Conventional soil fertilization methods often suffer from low efficiency due to nutrient immobilization, leaching, and volatilization. Foliar fertilization presents key advantages as it bypasses soil limitations but encounters obstacles such as leaf scorching and limited nutrient translocation1. Recent progress in bionanotechnology offers potential solutions by utilizing nanoparticles (NPs) with tailored properties to improve nutrient delivery to plant tissues. Comparably bigger than their ionic counterparts, yet small enough to penetrate all the relevant plant barriers e.g. cuticle, stomata, cell wall and vasculature, NPs can deliver plant mineral nutrients right where needed, overcoming the limitations of ions mobility and enhancing nutrient use efficiency1. However, unravelling the intricate fate and behavior of NPs within plants hampers the potential implementation of a nano-approach into foliar fertilization. Employing advanced bioimaging techniques can provide valuable mechanistic insights regarding plant interaction with and assimilation of NPs, which can positively contribute to our understanding and strengthen the case for nanotechnology adoption in plant production.
The objective of our research is to develop an NP-based system that allows for efficient delivery of Mn, one of the essential plant mineral nutrients, via foliar fertilization. To this end, formulation and NP physicochemical properties are optimized to enable effective penetration of the leaf surface, securing the delivery of adequate amounts of bioavailable Mn, whilst reducing the risk of scorching. At the same time, we want to characterize NP uptake pathways, distribution and assimilation of NPs in Mn-deficient barley plants. In this poster, we present a comprehensive investigation employing confocal imaging, nano-computed tomography (nano-CT) and laser-ablation inductively coupled plasma mass spectrometry (LA-ICP-MS) to elucidate the dynamics of foliar-applied NPs.
Methods
25 nm poly(acrylic acid)-coated Mn oxide (PAA-MnO) NPs were produced via one-pot polyol method2. NP physicochemical properties such as size, shape, surface charge, dissolution and Mn oxidation state, were characterized using different techniques, including dynamic light scattering, TEM, ICP-MS and XPS. Fluorophore-labelled (DiI-PAA-MnO) and Ce-spiked (Ce-PAA-MnO) NPs were produced for confocal and LA-ICP-MS applications, respectively.
Mn-deficient 21-day-old barley plants were used for the NP application experiments. To study the NP leaf uptake, fluorescent DiI-PAA-MnO NPs were imaged 2 to 5 hours after the leaf application using a confocal microscope (Leica Stellaris 8). A small portion of the dosed area was excised with a scalpel, placed on a microscope glass slide, and submerged into perfluorodecalin 95% (Sigma-Aldrich) before imaging.
The nano-CT experiments were performed at the European Synchrotron Radiation Facility id16b beamline in Grenoble (FR). For these, pristine PAA-MnO NPs were dosed on barley leaves. 5 hours after treatment, a small leaf cut was placed inside a 200 µL pipette plastic tip and mounted on top of

a rotating sample stage. The beamline was then set up in a projection geometry with a 29 keV pink beam focused to 50 x 50 nm². Each sample was scanned at four sample-to-detector distances with 900 angles over 360 degrees of rotation. The phase was retrieved using an iterative contrast transfer function (CTF) approach. Finally, the data was reconstructed and post-processed in Dragonfly, which was also used for visualizations.
For the LA-ICP-MS experiment, Ce-PAA-MnO were used. 5 hours after the application, a small portion of the leaf exposed area was cut, embedded in OCT mounting media and frozen in dry ice-cooled liquid hexane. The OCT molds were sliced at -30°C using a cryotome (Leica CM3050S) and freeze-dried overnight. Thin 14 µm cross-sections were ablated using a nanosecond LA unit (Iridia 193 nm excimer laser ablation system, Teledyne CETAC technologies).
Results
Our experiments document the early stages of NP uptake in plant leaves. Confocal analysis showed that NP uptake in barley leaves occur as early as two hours after the application and that stomata appear to be the main gateway for NP entry into the leaf. To validate the confocal imaging findings, nano-CT was used to study the uptake pathway of pristine PAA-MnO NPs. Nano-CT results corroborates the data obtained via confocal imaging, as NPs were detected inside the mesophyll below the stomata area. Despite nano-CT high resolution, NP clusters were visibile only when the leaf was pre-treated with a CaCl2 solution allowing for NPs aggregation inside the mesophyll. Finally, the correlation of nanoparticle distribution patterns observed via confocal imaging and nano-CT was determined by LA-ICP-MS, which confirmed the stomatal pathway as the main gateway for NP entry into the mesophyll, and highlighted the potential presence of NPs inside the leaf vascular tissue.
Conclusion
Our research highlights the strengths of three different, yet complementary, bioimaging techniques. Easy procedures for sample preparation and cellular resolution make CLSM a powerful technique to visualize NP uptake and distribution within plant cells and tissues. However, the imaging depth of confocal microscopy is limited to the superficial layer of the sample. Scattering, photobleaching and noise are few factors that restrict its use to study processes occurring a few hundred microns below the leaf surface. To overcome some of these issues, we integrated nano-CT imaging to obtain high-resolution, real three-dimensional images of pristine NP clusters inside the leaf. Complementing this, laser-ablation ICP-MS was used for elemental mapping, allowing us to study NP concentration gradients and NP spatial distribution at the whole leaf level. By combining these complementary techniques, we gained a comprehensive understanding of the processes occurring in the early hours after the leaf application of NPs.
This poster underscores the pivotal role of cutting-edge bioimaging techniques for unraveling the complex dynamics of foliar-applied NPs within plant systems, paving the way for the rational design and implementation of nanoparticle-based agricultural innovations.

Keywords
Manganese, nanoparticle, uptake, bioimaging

Reference:
1. Husted et al., 2023 – DOI: 10.1016/j.tplants.2022.08.017
2. Marasini et al., 2021 – DOI: 10.3390/app11062596

1236

Visualization of the Endosomal Fate of mRNA-Lipid Nanoparticles Reveals the Reason for Low Escape Rate

Dr. Anke Kaltbeitzel[1], Gunnar Glaßer[1], Dr. Johanna Simon[2], Dr. Eleni Samaridou[2], Dr. Moritz Beck-Broichsitter[2], Kai Speth[1], Prof. Dr. Volker Mailänder[1], Dr. Ingo Lieberwirth[1]
[1]MPI Polymer Research, Mainz, Germany, [2]Merck KGAA, Darmstadt, Germany

Poster Group 1

Background incl. aims
During Covid-19 pandemic, lipid nanoparticles (LNPs) have proven an indispensable drug for fighting viral infections[1]. They also bear potential as drugs against cancer and in many other fields[2]. They are formed of ionizable cationic lipids, helper lipids, PEGylated lipids and mRNA. They assemble at low pH during manufacturing, taking advantage of electrostatic interaction of cationic lipids with negative charges of the phosphate backbone of mRNA. The LNPs are taken up by cells into endosomes. Transfer of mRNA from the endosome to the cytosol is a prerequisite for the transcription of mRNA into drug effective proteins. Ionizable cationic lipids are thought to hold a crucial functional role because at low pH in late endosomes they should interact with and destabilize the endosomal membrane[3].
Despite vaccines being efficient, it is known that endosomal escape of mRNA is a bottle neck for this technology, being in the low percent range[4]. Visualization of endosomal processing of LNPs is crucial to understand the inefficiency of release.

Methods
Using correlative light and electron microscopy (CLEM) we were able to visualize the LNPs within endosomes for 2 different LNP formulations: lab scale LNPs with mRNA encoding for Firefly Luciferase and the COVID-19 vaccine Comirnaty® produced by Pfizer/Biontech. During administration to dendritic cells, the LNPs were exposed to an RNA stain to confer fluorescence for the correlation. Cells were incubated with LNPs for 6, 16-18 and 24h. Subsequently, cells were high pressure frozen (HPF), OsO4 and Uranyl-acetate stained, embedded in EPON and sectioned. Confocal images and EM images (SEM and TEM) were registered.

Results
After 6h incubation with lab scale LNPs, we see fluorescently stained particles of ~100nm size in endosomes on the verge of aggregation. After 16-18h the proportion of LNPs in endosomes has increased, coalescence took place resulting in dense layered structures. These structures clearly differ from endogenous multilamellar bodies but resemble TEM images of LNPs[5]. After 24h, endosomes are packed with large aggregates. Disentanglement of the dense stratified layers in some parts of the aggregates is observed. Despite filling > 90% of the endosomes, the aggregates rarely touch the endosomal membrane. However, at few places local ruptures of the endosomal membrane are visible.

Conclusion
We were able to visualize processing of LNPs in endosomes after uptake. We see massive accumulation of LNPs in endosomes over a time period of 24 hours, resulting in coalescence of LNPs. This process has rather been considered to limit the lifetime for storage of vaccine formulations. However, it also has crucial impact on endosomal escape. Release of mRNA is thought to occur via local breakup of the endosomal membrane after contact with cationic lipids followed by release of single LNPs to the cytosol[3]. Our images reveal a different scenario: PEGylation of LNPs minimizes contact with the endosomal membrane in early endosomes. Yet, coalescence of LNPs takes place due

to massive accumulation of LNPs in endosomes leading to concentrations orders of magnitude above those in the formulations. Coalescence also increases the density of PEG-groups on the surface, thus further reducing contact between LNP agglomerates and the endosomal membrane. Maturation of the endosomes causes a drop of pH so that ionizable cationic lipids get increasingly positively charged. This leads to electrostatic repulsion of the lipids resulting in the observed disentanglement of the lipid layers in the agglomerates. On the surface of the agglomerates there is local breakup of the lipid layers. Helped by their positive charge, loose strands locally interact with and perforate the endosomal membrane. However, the agglomerates are too bulky to pass through the membrane with their mRNA load and diffusion of single mRNA strands is hampered by their electrostatic attraction to the cationic lipids. Only a complete breakdown of the endosomes would reincrease the pH to levels allowing for efficient mRNA diffusion to the cytosol. Our findings indicate that the very concept of LNP assembly finally limits the mRNA release. Careful adjustment of the apparent pKa value of the ionizable cationic lipids can optimize the release rate.

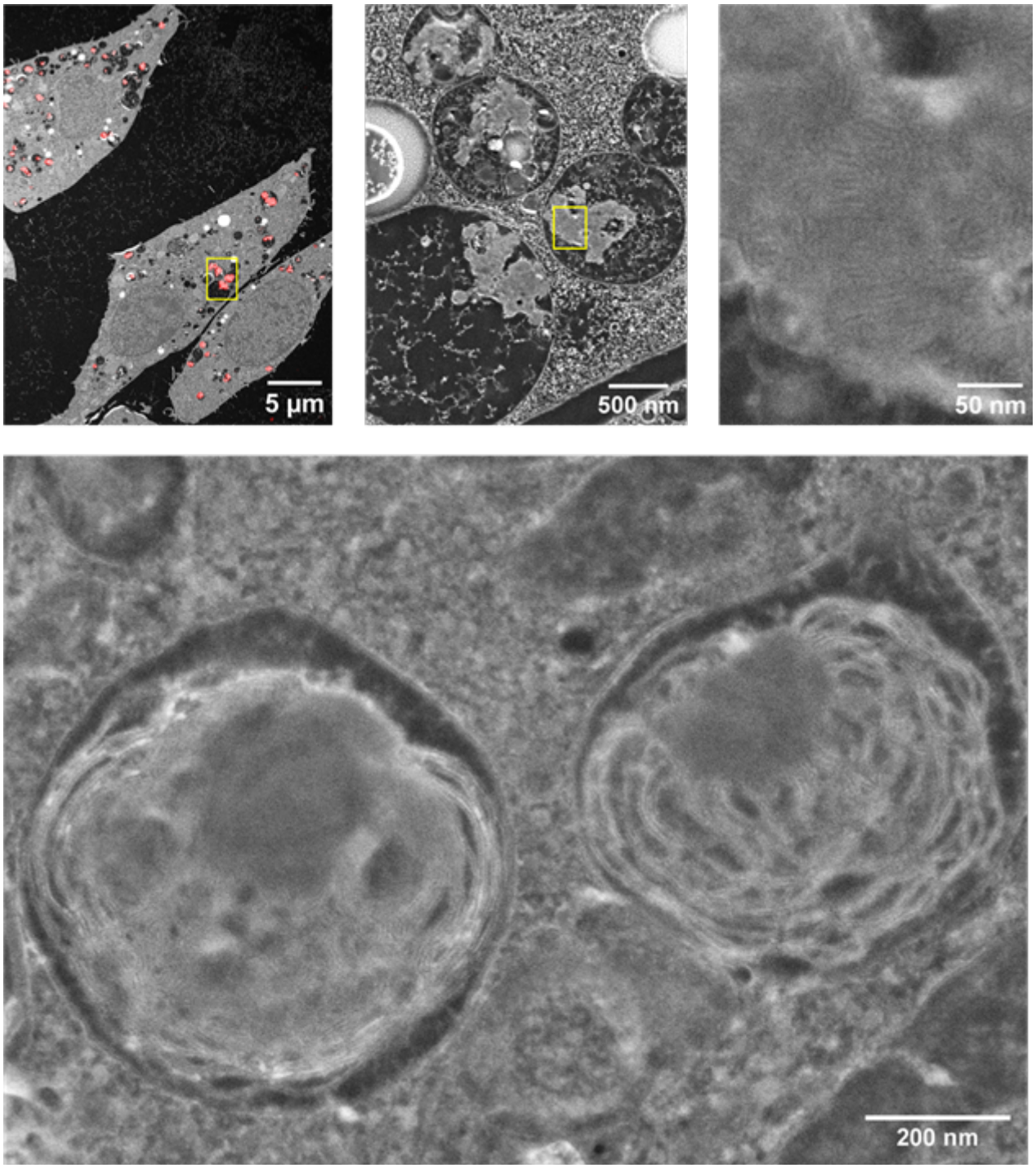

Keywords:

CLEM, Lipid Nanoparticles, Endosomal Escape

Reference:

[1] Schoenmaker L, Witzigmann D, Kulkarni JA, Verbeke R, Kersten G, Jiskoot W, Crommelin DJA. mRNA-lipid nanoparticle COVID-19 vaccines: structure and stability. Int J Pharm. (2021), 601:120586, doi:10.1016/j.ijpharm.2021.120586
[2] Mitchell, M.J., Billingsley, M.M., Haley, R.M. et al. Engineering precision nanoparticles for drug delivery. Nat Rev Drug Discov (2021), 20, 101–124, doi: 10.1038/s41573-020-0090-8
[3] Gyanani, V., Goswami, R. Key Design Features of Lipid Nanoparticles and Electrostatic Charge-Based Lipid Nanoparticle Targeting. Pharmaceutic (2023) 15, 1184, doi: 10.3390/pharmaceutics15041184.
[4] Kim J., Eygeris Y., Gupta M., Sahay G. Self-assembled mRNA vaccines. Advanced Drug Delivery Reviews (2021) ,170, 83–112, doi: 10.1016/j.addr.2020.12.014
[5] Szebeni J., Kiss B., Bozó T., Turjeman K., Levi-Kalisman Y., Barenholz Y., Kellermayer M. Insights into the Structure of Comirnaty Covid-19 Vaccine: A Theory on Soft, Partially Bilayer-Covered Nanoparticles with Hydrogen Bond-Stabilized mRNA–Lipid Complexes. ACS Nano (2023), 17 (14), 13147-13157, doi:10.1021/acsnano.2c11904

1257

Correlative light electron microscopy for improved investigation of subcellular GLUT4 distribution in human skeletal muscle

PhD student, MSc Kaspar Wredstrøm Persson[1], Christian T. Voldstedlund[1], Chris Neal[3], Judith M. Mantell[2,3], Erik, A. Richter[1], Paul Verkade[2], Thomas E. Jensen[1]
[1]August Krogh Section for Molecular Physiology, Department of Nutrition Exercise and Sports, University of Copenhagen, Copenhagen, Denmark, [2]School of Biochemistry, University of Bristol, Bristol, UK, [3]Wolfson Bioimaging Facility, University of Bristol, , UK

Poster Group 1

Background incl. aims
Insulin stimulated glucose uptake into skeletal muscle tissue is facilitated by translocation of the Glucose Transporter Type 4 (GLUT4) from intracellular storage sites to the cell surface, a well-established site of impairment in obesity linked insulin resistance. Despite impaired GLUT4 translocation, canonical signal transmission via the Insulin receptor substrate-1 is frequently observed to be normal, and human fractionation studies indicate that intracellular GLUT4 is missorted in individuals with insulin resistance. Exercise acutely promotes skeletal muscle glucose uptake by insulin-independent GLUT4 translocation and improves skeletal muscle insulin sensitivity independent of present insulin resistance in the hours following exercise - a phenomenon coexisting with the redistribution of GLUT4 to well-known insulin responsive subcellular compartments in metabolically healthy individuals. Whether the subcellular localization of GLUT4 is distorted in obesity linked insulin resistance and is corrected by a single insulin-sensitizing bout of exercise has not yet been investigated by high resolution microscopy-based approaches.
The aims of this study were 1) to establish and apply a quantitative correlative light electron microscopy (CLEM) workflow on human skeletal muscle biopsies, and 2) to investigate the subcellular distribution of GLUT4 in skeletal muscle single fibers of metabolically healthy vs. insulin resistant individuals prior to, immediately after and 3 hours into recovery from a single exercise bout.

Methods
Skeletal muscle biopsies were obtained from m. Vastus Lateralis of normal weight (BMI: 22.8 ± 1.7) and obese (BMI: 36.2 ± 3.1) young men (age 25-35y) (n=5) before, immediately after, and 3 hours into recovery from an acute bout of bicycling exercise (65% VO2max, 30 min). Immediately after excision, biopsies were chemically fixed for light and electron microscopy. Muscle fiber bundles were teased apart to single fibers, labelled with a GLUT4 antibody and subsequently FluoroNanogold, counterstained with Hoechst, embedded in agar on a glass slide, sealed with a coverslip and imaged using a Leica SP8 confocal microscope equipped with a 40x oil objective. For each muscle fiber, a full fiber surface tile scan was obtained using transmitted light followed by a single-tile 10µm z-stack for the wavelengths of interest. The specific tile was chosen based on visual landmarks (bends, curves, non-fiber substances etc.) for optimal recognition of the area in the subsequent electron microscopy imaging. Following gentle removal of the coverslip, in-agar fibers were further processed directly on the glass slide for electron microscopy. The procedure included silver enhancement of the FluoroNanogold particles, chemical post-fixation, lipid and nucleic acid staining and graded resin infiltration and polymerization. The specific areas of interest from confocal imaging were identified under a stereomicroscope and targeted for in-resin ultrathin (70 nm) sectioning. The sections were mounted on grids and imaged on a Tecnai T20 transmission electron microscope. Tile imaging was performed blinded along the edges of the fiber prior to low-magnification, full-section overview imaging. Overview images containing bleached areas were used in combination with confocal and stereomicroscope images to overlay the corresponding light and electron microscopy images and confirmed by the shape, size and distance between nuclei.

Results
Insulin resistance was confirmed in participants with obesity both in the fasting state by the homeostasis model assessment 1 of insulin resistance (HOMA1-IR) (obese: 3.7 ± 2.1 vs. lean: 0.7 ± 0.1, p=0.02) as well as in response to an oral glucose tolerance test by the Matsuda Index (obese: 3.4 ± 1.5 vs lean: 15.7 ± 3.6, p=0.0001). The CLEM workflow was successfully implemented, and data are currently being analysed for the accumulation of GLUT4 in various subcellular compartments prior to, immediately after, and 3 hours into recovery from a single insulin-sensitizing bout of exercise.

Conclusion
In this study, we successfully established a novel quantitative CLEM workflow to investigate the subcellular distribution of GLUT4 in human skeletal muscle fibers with high spatial precision, achieving resolution down to the nanometer scale while ensuring ultrastructural integrity. Our methodology enabled detailed information on the localization of GLUT4 in single muscle fibers from both metabolically healthy and insulin-resistant individuals, and ongoing analyses aim to elucidate whether insulin resistance is associated with distorted subcellular distribution of GLUT4 and whether this is corrected by a single bout of exercise. This research advances our understanding of GLUT4 dynamics and provides a foundation for potential therapeutic strategies targeting insulin resistance through exercise. Moreover, this advanced imaging approach can be utilized to investigate various other subcellular processes in muscle tissue, expanding its applicability in muscle biology research.

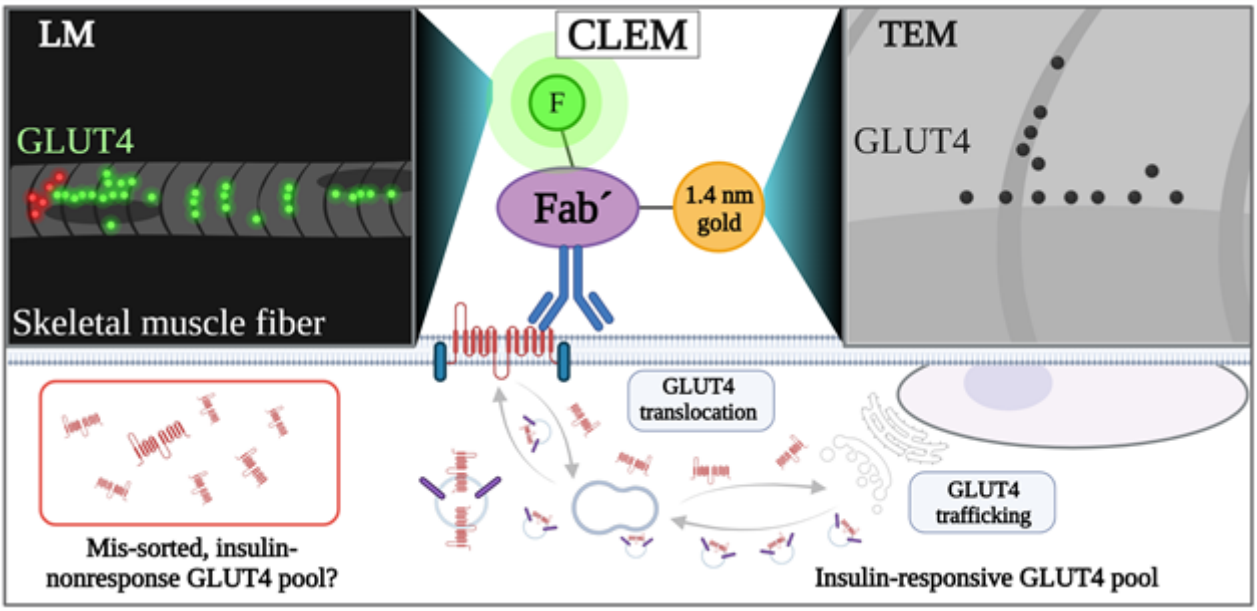

Keywords:

muscle, GLUT4, insulin, exercise, CLEM

Reference:

James, D. E., Stöckli, J. & Birnbaum, M. J. The aetiology and molecular landscape of insulin resistance. Nat. Rev. Mol. Cell Biol. 22, 751–771 (2021).

Garvey, W.T. et al. Evidence for defects in the trafficking and translocation of GLUT4 glucose transporters in skeletal muscle as a cause of human insulin resistance. J Clin. Invest. 101, 2377-2386 (1998)

Sylow, L., Kleinert, M., Richter, E. A. & Jensen, T.E. Exercise-stimulated glucose uptake – regulation and implications for glycaemic control. Nat. Rev. Endocrinol. 13, 133-148 (2017)

Knudsen, J. R. et al. Prior exercise in humans redistributes intramuscular GLUT4 and enhances insulin-stimulated sarcolemmal and endosomal GLUT4 translocation. Mol Metab 39, (2020).

Tanner, H., Sherwin, O & Verkade, P. Labelling strategies for correlative light electron microscopy. Microsc Res Tech. 86, 901-910 (2023)

1275

Embryonic and postembryonic development of arthropods: imaging from the cellular to the whole organism level

Polona Mrak[1], Urban Bogataj[1], Katja Kunčič[1], Žiga Fišer[1], Miloš Vittori[1], Nada Žnidaršič[1]
[1]University of Ljubljana, Biotechnical Faculty, Department of Biology, Ljubljana, Slovenia

Poster Group 1

Background

Knowledge of arthropod development is important for understanding morphogenesis, comparative embryology and the application of these concepts in various fields of bioscience. The processes of morphogenesis and differentiation during embryonic and postembryonic development of an organism are complex and interdependent at all organisational levels, which is crucial for the establishment of the functions of individual organs. The analyses of samples of isolated organs and of intact animals complement each other, particularly in terms of understanding the 3D structure at different levels, and require the combined use of complementary imaging techniques: micro-computed tomography (micro-CT), histology, fluorescence labelling and various electron microscopy methods, including array tomography (AT) and transmission electron microscopy (TEM) tomography. In addition, the study of developmental processes demands the analysis of temporally sequential developmental stages, which range in duration from a few hours to a few days. The basis for an integrative study of developmental processes is the establishment of a staging system for the species investigated. Accordingly, the first aim of our studies is to comprehensively characterise the morphology of the developmental stages in the investigated crustacean species. Next, in the context of comparative studies of arthropod development we aim to study morphogenesis of the digestive system and the integument in detail, focusing on the differentiation of epithelia, that is crucial for shaping of the organ and establishment of vital functions.

Methods

The morphological characterization of developmental stages in the crustacean species (Porcellio scaber and Asellus aquaticus) was performed by imaging of living organisms (embryonic and postembryonic stages) by light microscopy and fluorescence labelling of cell nuclei in fixed whole-mount embryos. To study morphogenesis of selected organs and differentiation of epithelia, the samples of P. scaber mid- and late-stage embryos, postembryonic stages (marsupial and postmarsupial mancae) and adults were analysed using micro-CT, histology, fluorescence labelling of selected structures and electron microscopy. For micro-CT imaging whole animals were chemically fixed and dried, and after imaging the segmentation of the digestive system was performed. Histological and ultrastructural analysis were performed on semithin and ultrathin sections, respectively, prepared from chemically fixed, dehydrated and resin-embedded samples of whole organisms or isolated organs.

Results and conclusions

Morphological analysis of sequential developmental stages is currently being used to characterise embryonic development of a freshwater crustacean A. aquaticus, a model organism in various fields, notably ecotoxicology and evolutionary ecology. The morphological characteristics of intact embryos and mancae (postembryonic stages) were analysed by light microscopy each day of the development. Fluorescence labelling of nuclei is particularly suitable for the analysis of early embryonic development, when the arrangement of cells follows a well-defined pattern (Fig. 1A). According to the main morphological modifications, the development of A. aquaticus was divided into 10 embryonic stages, the stage of marsupial manca and the stage of postmarsupial manca (Fig. 1B, C). During the formation of the integument, gut and digestive glands the differentiation of epithelial

tissues was described in P. scaber, including changes in cell shape and ultrastructure. Using micro-CT, we obtained 3D morphology data of the digestive system in intact organisms of distinct developmental stages (Fig. 2A). Data on the changes in epithelial cell shapes in different organs during development were obtained by analysing semithin sections (Fig. 2B). The elongation of the invaginated foregut and hindgut until they fuse into a single digestive tube and the gradual incorporation of the yolk into the developing digestive glands in embryos, as well as the differentiation of the gut regions in postembryonic stages, were clearly visible. At the ultrastructural level, the processes of cell junction differentiation, apical and basal plasma membrane remodelling, and apical extracellular matrix (cuticle) formation were characterised by transmission electron microscopy (Fig. 2C), supplemented with AT for the 3D context of the cell junctions. The combination of the described imaging analyses provides a broad spectrum of information on the structure of individual cells, tissues and whole organs at the same developmental stage in the context of the whole organism. This allows us to relate modifications in detailed cell ultrastructure and tissue differentiation to morphogenetic processes at the organ and organism level during development.

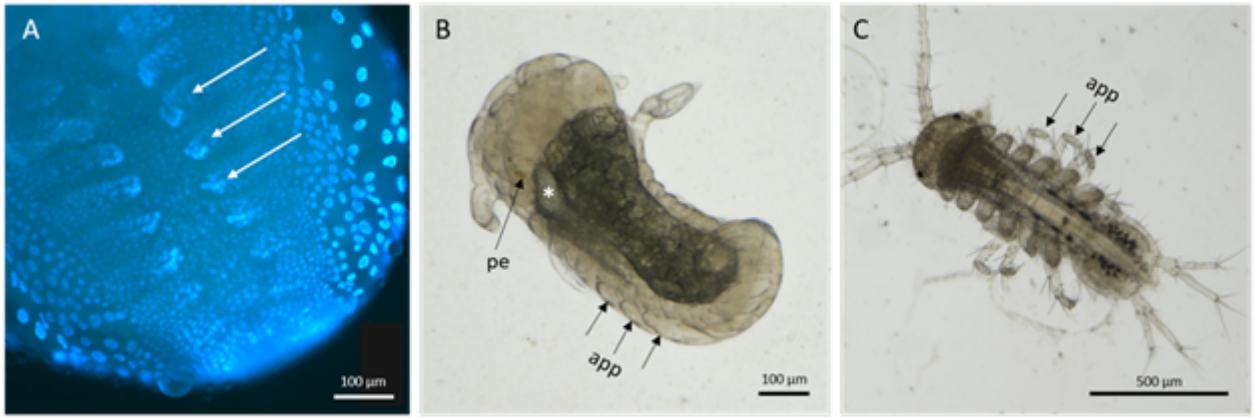

Figure 1: Imaging of developmental stages in crustaceans. (A) Fluorescence labelling of cell nuclei with DAPI shows formation of body segments and limb buds in germ band (white arrows) of *P. scaber* early embryo. (B) Imaging of intact late embryo of *A. aquaticus* reveals elongation of appendages under the egg envelope (app), eye pigmentation (pe) and yolk inclusion in the digestive glands (white asterisk). (C) Postembryonic stages of *A. aquaticus* are identified by release of appendages (app) and locomotion of animal.

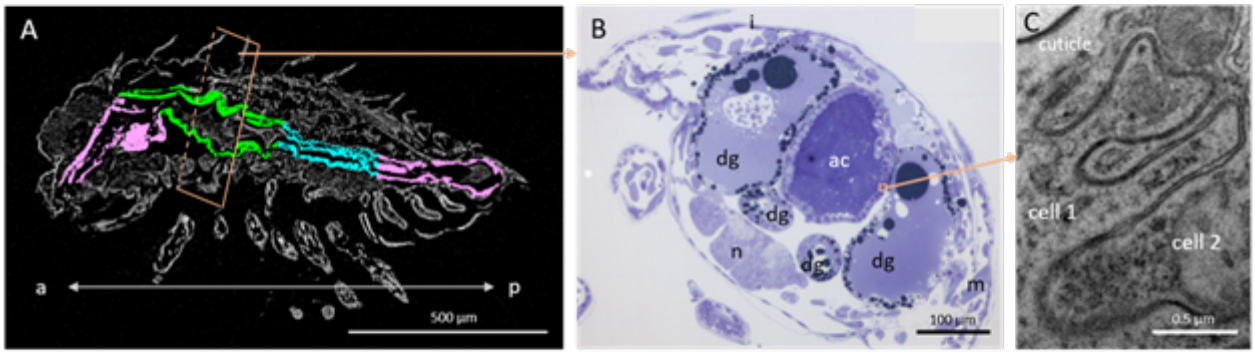

Figure 2: Imaging of gut morphogenesis in *P. scaber* postembryonic stage from whole animal level to ultrastructural level. (A) Micro-CT virtual longitudinal section of whole animal with segmented gut regions, from anterior (a) to posterior (p): foregut, anterior chamber, papillate region, rectum. (B) Cross section of an animal through the anterior part shows distribution of organs and the shape of epithelial cells: two pairs of digestive glands (dg), anterior chamber with simple epithelium (ac), integument with exoskeleton (i), skeletal muscles (m), nerve tissue (n). (C) Ultrastructure of septate junction between two neighbouring epithelial cells in the gut.

Keywords:

arthropod development, micro-CT, histology, TEM

1282

Correlative X-ray and Electron Microscopy Workflow for Investigating Grey Matter Lesions in Multiple Sclerosis

PhD Alexandra Glasmacher-Kober[1], Susann Hesse[1], Prof. Dr. Fred Wouters[1], Dr. Gertrude Bunt[1]
[1]Research Unit Innovative Microscopy Technologies, Institute for Neuropathology, University Medical Center Goettingen, Goettingen, Germany

Poster Group 1

Background: Multiple sclerosis (MS) is a complex neurological disease characterized by a heterogeneous distribution of lesions within the brain, making their investigation challenging. Currently, the treatment of MS primarily focusses on white matter pathology. However, it is increasingly recognized that injuries in the cortex, i.e. grey matter lesions, play a critical role in progressive disease outcome. Unfortunately, these grey matter lesions are poorly understood. In order to gain a better understanding of these lesions and their underlying pathological mechanisms, we pursue an ultrastructural study. We have established a correlative microscopy workflow that combines X-ray microscopy (XRM) and electron microscopy (EM). This workflow enables us to track and analyse the diseased regions in human brain samples throughout the different stages of tissue preparation up to their ultrastructural investigation.

Methods: we apply a correlative multiscale approach based on XRM, scanning electron microscopy, and transmission electron microscopy to analyse MS lesions in human brain samples.

Results: XRM is used to identify the diseased regions during the tissue preparation process for ultrastructural imaging, starting from fixed brain tissue to the final EM samples. Through XRM, we are able to identify lesions in the brain samples. Using a coordinate system, specific regions of interest within resin-embedded EM samples are then targeted for detailed ultrastructural examination by electron microscopy. This targeted approach enables us to directly visualize and analyse the ultrastructural changes of grey matter lesions.

Conclusion: The combination of X-ray microscopy (XRM) and electron microscopy (EM) offers a systematic approach for analysing the spatial distribution and the ultrastructural changes of heterogeneously localized diseased areas.

Keywords:

correlative microscopy, XRM, EM, neuropathology